

A precise asymptotic analysis of learning diffusion models: theory and insights

Hugo Cui¹, Cengiz Pehlevan^{2,3,4}, and Yue M. Lu^{1,4}

¹Center of Mathematical Sciences and Applications, Harvard University

²Center for Brain Science, Harvard University

³Kempner Institute for the Study of Natural and Artificial Intelligence, Harvard University

⁴John A. Paulson School of Engineering and Applied Sciences, Harvard University

Abstract

In this manuscript, we consider the problem of learning a flow or diffusion-based generative model parametrized by a two-layer auto-encoder, trained with online stochastic gradient descent, on a high-dimensional target density with an underlying low-dimensional manifold structure. We derive a tight asymptotic characterization of low-dimensional projections of the distribution of samples generated by the learned model, ascertaining in particular its dependence on the number of training samples. Building on this analysis, we discuss how mode collapse can arise, and lead to model collapse when the generative model is re-trained on generated synthetic data.

Diffusion and flow-based generative models represent a new paradigm in the sampling of high-dimensional probability densities. Such methods operate by recasting the sampling problem as a transport from a simple base distribution to the target density. The velocity field directing the transport can further be parameterized by a neural network, and learnt from data [57, 58, 28, 26]. These ideas have been successfully implemented in a number of algorithmic frameworks [58, 38, 2, 39, 59], with applications ranging from image generation [44, 47, 52] to drug discovery [67].

The surprising effectiveness of such models in learning probability densities in high dimensions hints at the presence of *architectural biases* built in the network parametrization, placing strong priors on the class of densities that can be generated by the model. When aligned with the target density, these architectural biases can allow generative models to learn a good approximation of the target from only a small number of training samples [27]. Naturally, when the biases are ill-suited to the task, they can also lead to poor solutions. Gaining a solid theoretical understanding on how the neural network architecture shapes the generated density is hence a central, yet still largely open, research question.

Arguably, the prominent technical obstruction lies in the need to reach a *precise* characterization of the density a given architecture learns to generate. A large fraction of theoretical studies of generative models [14, 11, 5, 32, 33, 35] analyze only the generative transport process, starting from the assumption that a L^2 -accurate approximation of the velocity or score is available. This gap has in part been filled by a recent line of works [41, 12, 4, 10], which establishes that some target densities can provably be learnt by neural networks, provided sufficient width and number of samples. Such sample complexity bounds are however little descriptive of the shape of the generated density, nor do they capture biased failure cases where the architecture is not expressive enough to yield a good approximation. Closer to our work, authors of [16] conduct a tight analysis of a simple generative model, which is however limited to the highly stylized case of a binary Gaussian mixture target density with isotropic covariances. The present manuscript overcomes these barriers, and provides a *sharp* characterization of the generated distribution for models learning from structured target densities.

Main contributions

We consider generative models parametrized by a two-layer Denoising Auto-Encoder (DAE) with tied weights and trainable skip connection, trained with online Stochastic Gradient Descent (SGD), in the framework of stochastic interpolation [2, 3]. We consider target distributions corresponding to (possibly infinite) Gaussian mixtures in high dimensions, with generic cluster covariances, and centroids lying on a low-dimensional manifold – reflecting a pervasive intuition in machine learning [60, 68]. Overcoming previous limitations, we derive a *tight* asymptotic description of the generated distribution. More precisely,

- We provide a tight characterization of the training dynamics in terms of a set of deterministic Ordinary Differential Equations (ODEs), bearing over a finite set of low-dimensional summary statistics.

- Building on these results, we similarly provide a tight low-dimensional characterization of the generative transport process, thereby reaching a sharp description of low-dimensional projections of the generated density, as a function of the number of samples and sampling time. The theoretical predictions further quantitatively capture experiments on simple real datasets.
- We discuss and illustrate how a phenomenon akin to mode collapse [25] can arise, and lead to a loss of diversity in the generated density. Iterating and extending over our analysis to cases where the generated data is further re-used to train the generative model, we highlight how this mode collapse ultimately conduces to model collapse [55].

The code employed in this manuscript is accessible on [this online repository](#).

Related works

Sampling accuracy and dynamics– A large body of works on diffusion-based and flow-based generative models has been devoted to the study of the generative process, assuming access to a L^2 -accurate score estimate, or to the exact empirical score. [14, 11, 5, 32, 33, 35, 6, 13, 18, 34] provide rigorous bounds on appropriate distances between the target and generated probability distributions. The sequential emergence of structure in the transported density with sampling time has been investigated in [8, 7, 54, 53, 1, 64, 36], evidencing the presence of rich critical phenomena. [23] explore the computational hardness of sampling for an array of graphical models.

Sample complexity bounds– Complementing this set of results, a recent stream of work refined these bounds by further ascertaining the *sample complexity* required to learn accurate score estimates [9, 30, 69, 20, 72]. For data distributions close to the one considered in the present work, [22, 15] show how the score of Gaussian mixture densities can be learnt algorithmically in efficient fashion. Similarly, for target densities with latent low-dimensional structure, [41, 12, 10] prove that DAE-parameterized models are able to learn the latent structure, and thus break the curse of dimensionality. None of these bounds, however, allow for an precise description of the *geometry* of the generated density. Furthermore, because such results primarily focus on settings where the target densities can be provably learned by the model with enough samples, they are not descriptive of unrealizable settings where the model is unable of perfect learning, and thus overlook possible failure modes and biases.

Tight characterization of learning in AEs– In order to study such cases, *sharper* results are warranted. In this direction, a sizeable research effort has been devoted to analyzing the learning of AEs [62, 61], arguably the simplest instance of the class of denoiser neural networks used in generative models. The learning dynamics of AEs under (S)GD was characterized in [43] in the linear case, and [45] for non-linear models. [17] derive a tight asymptotic characterization of the learning of AEs for a denoising task, reaching a precise description of the generated density when this network is used to parametrize a generative model [16]. This characterization is however limited to a rather stylized target density, namely a binary Gaussian mixture with isotropic clusters, and thus fails to describe real data distributions. The present manuscript overcomes this barrier, and considers realistically structured target densities.

Inductive bias in generative models– Even with moderately large training sets, generative models succeed in generating novel images, rather than reproducing memorized training samples [71, 70, 49, 42, 66, 37, 21, 65]. This surprising efficiency strongly hints at the presence of inductive bias inherited from the network parametrization, nudging the model towards good solutions. The inductive bias of U-net architectures [48] has been investigated in [27], who observe how these architecture tend to learn relevant harmonic bases. In a similar spirit, the concurrent work of [29] evidences how the bias of such convolutional architectures towards learning equivariant and local scores helps to promote good solutions. Finally, [40] demonstrates that U-nets are closely related to message-passing algorithms on random hierarchical data, and thus particularly adapted to such structure.

1 Problem formulation

We start by providing a succinct overview of the problem of sampling a target density ρ over \mathbb{R}^d using ideas from generative transport. For definiteness and ease of presentation, we consider in this manuscript the class of stochastic interpolant models [2], which shares substantial connections with other methods, including score-based diffusion models [59] and denoising methods [28, 26].

Sampling– A sample $X_1 \sim \rho$ can be obtained from a Gaussian sample $X_0 \sim \mathcal{N}(0, \mathbb{I}_d)$ by evolving the latter for $t \in [0, 1]$ with the Stochastic Differential Equation (SDE)

$$\frac{dX_t}{dt} = \left(\dot{\beta}_t - \frac{\dot{\alpha}_t}{\alpha_t} \beta_t + \epsilon_t \frac{\beta_t}{\alpha_t^2} \right) f(t, X_t) + \left(\frac{\dot{\alpha}_t}{\alpha_t} - \frac{\epsilon_t}{\alpha_t^2} \right) X_t + \sqrt{2\epsilon_t} dW_t, \quad (1)$$

where W is a Wiener process. This statement holds for any choice of interpolants $\alpha, \beta \in \mathcal{C}^2([0, 1])$, $\epsilon \in \mathcal{C}^0([0, 1])$ provided $\alpha(0) = \beta(1) = 1$, $\alpha(1) = \beta(0) = 0$ and $\alpha(t)^2 + \beta(t)^2 > 0$, $\epsilon(t) \geq 0$ at all times $t \in [0, 1]$ [2]. In (1), the function $f : [0, 1] \times \mathbb{R}^d \rightarrow \mathbb{R}^d$ is defined as

$$f(t, x) = \mathbb{E}[x_1 | \alpha_t x_0 + \beta_t x_1 = x], \quad (2)$$

with the conditional expectation bearing over $x_1 \sim \rho$, $x_0 \sim \mathcal{N}(0, \mathbb{I}_d)$. Intuitively, $f(t, x)$ can be interpreted as a *denoising function*, which aims to recover the sample x_1 from the interpolated version $\alpha_t x_0 + \beta_t x_1$, in which it is corrupted by the noise x_0 .¹ Perhaps then unsurprisingly, the function f admits a natural characterization as the minimizer of the quadratic denoising objective

$$\mathcal{R}[f] = \int_0^1 \mathbb{E} \|f(t, \alpha_t x_0 + \beta_t x_1) - x_1\|^2 dt. \quad (3)$$

This formulation provides an opportune pathway to learn the function f governing the sampling (1) directly *from data*. The learning can be carried out following the usual machine learning rationale of (a) parametrizing f by a denoiser neural network and (b) replacing the expectation in (3) by an empirical average over a training set.

Architecture– In the present manuscript, following [17], we consider the simplest instance of denoising neural network, namely a two-layer DAE

$$f_{b,w}(x) = b \times x + \frac{w}{\sqrt{d}} \sigma \left(\frac{w^\top x}{\sqrt{d}} \right), \quad (4)$$

with activation function σ , and trainable skip connection $b \in \mathbb{R}$. For simplicity, we assume that the decoder and encoder are *tied*, namely parametrized by a unique set of weights $w \in \mathbb{R}^{d \times r}$. This assumption allows for a more concise exposition of the technical results, and was not found to sensibly alter the phenomenology of the model. We discuss in Appendix A how the analysis can be extended to generically untied weights. Further note that, importantly, the DAE (4) does not take the time t as an input. We detail in Appendix A how a time encoding scheme can be included in the analysis to reflect more practical schemes. On the other hand, experimentally, we did not find the inclusion of such an encoding to lead to qualitatively different learning behaviors.

Let us briefly situate the class of DAEs (4) with respect to models considered in related works. [12, 41] consider deep networks with ReLU activations, and sparsity constraints on the weights. Closer to our work, [10] similarly assume shallow AEs, but place themselves in the limit of infinite width ($r \rightarrow \infty$). On the opposite end of the spectrum, [16] consider shallow AEs with a single hidden unit ($r = 1$), and sigmoidal activations σ . The architecture (4) considered in the present manuscript, on the other hand, corresponds to finite width networks with arbitrary activations.

Training– The neural network (4) can now be used to parametrize the denoising function f in the objective (3). We consider training the DAE (4) with *online (single-pass) SGD*, with learning rate η and weight decay λ :

$$b_{\mu+1} - b_\mu = -\frac{\eta}{d^2} \left(\partial_b \mathbb{E}_t \left\| x_1^\mu - f_{b_\mu, w_\mu}(\alpha_t x_0^\mu + \beta_t x_1^\mu) \right\|^2 \right), \quad (5)$$

$$w_{\mu+1} - w_\mu = -\eta \nabla_w \mathbb{E}_t \left\| x_1^\mu - f_{b_\mu, w_\mu}(\alpha_t x_0^\mu + \beta_t x_1^\mu) \right\|^2 - \eta \frac{\lambda}{d} w_\mu. \quad (6)$$

The expectation \mathbb{E}_t over t bears over the uniform distribution over $[0, 1]$, or any approximation thereof by a chosen set of points $\mathcal{G} = \{t_1, t_2, \dots\}$. The updates (5) are iterated n times from a given initialization b_0, w_0 . Note that in online SGD, a fresh pair of samples $x_1^\mu \sim \rho$, $x_0^\mu \sim \mathcal{N}(0, \mathbb{I}_d)$ is employed at each training step, and the number of training steps

¹Note that the denoising function f is related to the score function s of the density of $\alpha_t x_0 + \beta_t x_1$ by the simple linear relation $\alpha_t^2 s(t, x) = \beta_t f(t, x) - x$.

thus coincides with the number of samples. Finally, it will prove convenient to introduce the training time $\tau = 2\eta n/d$, a quantity that remains finite in the asymptotic limit considered, which we detail below. We accordingly denote by b_τ, w_τ the values of the skip connection and weights at the end of training.

After training, the optimized DAE (4) f_{b_τ, w_τ} can then be employed in the generative flow (1) as a proxy for the true denoising function f :

$$\frac{dX_t}{dt} = \left(\dot{\beta}_t - \frac{\dot{\alpha}_t}{\alpha_t} \beta_t + \epsilon_t \frac{\beta_t}{\alpha_t^2} \right) f_{b_\tau, w_\tau}(X_t) + \left(\frac{\dot{\alpha}_t}{\alpha_t} - \frac{\epsilon_t}{\alpha_t^2} \right) X_t + \sqrt{2\epsilon_t} dW_t. \quad (7)$$

The SDE (7) can then be used for sampling. Because the learning is generically imperfect due to limited data and architectural bias, we generically have $f_{b_\tau, w_\tau} \neq f$, and thus the generated density $\hat{\rho}_\tau(t)$ –namely the law of X_t – differs from the target density ρ , even as $t \rightarrow 1$. One of the primary objectives of this work is to give a sharp asymptotic characterization of $\hat{\rho}_\tau(t)$.

Target density– In this manuscript, we consider target densities given by a (possibly infinite) Gaussian mixture supported on a latent low-dimensional manifold. Namely,

$$\rho = \int_{\mathbb{R}^\kappa} \mathcal{N}(\mu(c), \Sigma(c)) d\pi(c). \quad (8)$$

In words, the centroids $\mu(c) \in \mathbb{R}^d$ of the different clusters lie on a κ –dimensional manifold, equipped with a coordinate system $c \in \mathbb{R}^\kappa$. The distribution of the clusters on the manifold is given by the relative weights $\pi(c)$. Finally, each cluster can exhibit a non-trivial covariance structure $\Sigma(c) \in \mathbb{R}^{d \times d}$. For the analysis, we further assume that all the covariances $\{\Sigma(c)\}_c$ are jointly diagonalizable, and admit well-defined spectral densities ν_c in the high-dimensional limit $d \rightarrow \infty$. The density (8) reflects and models the celebrated *data manifold hypothesis* [60, 68], which posits that real data distributions lie on low-dimensional manifolds.

Let us mention that [41, 12, 10] similarly consider linear subspaces embedded in high dimensions, which can be viewed as special instances of (8) in the limit of vanishing covariances $\Sigma(c) = 0$ for all $c \in \mathbb{R}^\kappa$. Note also that Gaussian mixture distributions considered in e.g. [16] correspond to the special case of (8) where the cluster distribution π is a sum of K Dirac deltas, with K the number of clusters. To give a final example of a distribution falling in the class (8), let $\kappa = 2$, $\Sigma(c) = 0$ and $\pi = \mathcal{U}([0, 2\pi] \times [-1, 1])$, while $\mu(c) = (c_1 \cos c_1, c_1 \sin c_1, c_2, 0, \dots, 0)$. This corresponds to a swiss-roll distribution embedded in d dimensions. (8) thus allows to capture distributions with non-trivial latent structure.

High-dimensional limit– We aim at characterizing the generated density $\hat{\rho}_\tau(t)$ in the asymptotic limit of large data dimension and commensurably large number of samples, namely $d, n \rightarrow \infty$ with $n/d = \Theta_d(1)$. This asymptotic limit captures the non-trivial regime where the number of samples is not small enough for the neural network to trivially overfit, and conversely not infinite – thus allowing the investigation of finite data effects. We further suppose that the number of hidden units r of the DAE and the intrinsic dimensionality of the data manifold κ , alongside all other parameters, remain finite: $r, \kappa, \lambda, \eta = \Theta_d(1)$. Moreover, the diameter of the mixture (8) is also supposed to remain finite, i.e. there exist $D = \Theta_d(1)$ such that $\|\mu(c)\|_2 \leq D$ with probability 1 for $c \sim \pi$. Finally, we assume that the ambient dimension of the manifold is also finite, namely $\dim \text{span}(\{\mu(c)\}_c) = \Theta_d(1)$.

2 Precise characterization of the generated density

We are now in a position to detail our main technical findings, namely a sharp asymptotic characterization of the generated density $\hat{\rho}_\tau$ obtained from the sampling process (7), governed by the DAE f_{b_τ, w_τ} (4) trained with online SGD (5). Because it is challenging to describe a high-dimensional probability distribution, we rather aim at characterizing low-dimensional projections thereof. Formally, let us fix a reference space $\mathcal{E} \subset \mathbb{R}^d$ with finite dimensionality $R = \Theta_d(1)$, and let $E \in \mathbb{R}^{d \times R}$ be a matrix whose columns form an orthonormal basis of \mathcal{E} . We aim at a sharp characterization of the law $\Pi_{\mathcal{E}} \hat{\rho}_\tau(t)$ of the projection $E^\top X_t$ of a generated sample $X_t \sim \hat{\rho}_\tau(t)$. In words, the subspace \mathcal{E} corresponds to an observation space of interest, chosen by the statistician. Natural choices consists in electing a subspace where the target density exhibits non-trivial structure, with a view to probing how well it is reproduced at the level of the generated density – for example, the space spanned by the directions of larger variance of the target density ρ , or the space spanned by the latent manifold $\text{span}(\{\mu(c)\}_c)$.

The derivation of this characterization proceeds in two steps. First, we derive a sharp asymptotic characterization of the high-dimensional training dynamics induced by SGD (5). More precisely, we describe the evolution of a set of

low-dimensional summary statistics of the weights w over training time in terms of a collection of limiting ODEs. These summary statistics encode all the geometric information on w necessary to reach, in a second step, a sharp asymptotic characterization of the generative SDE (1) in terms of low-dimensional processes. Finally, this characterization yields a sharp description of $\Pi_{\mathcal{E}} \hat{\rho}_{\tau}(t)$ as a corollary.

2.1 Analysis of the learning

Our first result shows that the evolution under the SGD dynamics (5) of a set of summary statistics of the weights w of the DAE (4) is asymptotically described by a collection of deterministic limiting ODEs.

Result 2.1. (SGD dynamics) *Let $\tau > 0$ be a the training time, and w_{τ} be the weight matrix obtained from the stochastic SGD dynamics (5) from an initialization w_0 . The summary statistics $\mathcal{Q}_{\tau} \in \mathbb{R}^{r \times r}$, $Q_{\tau} : \mathbb{R}^{\kappa} \rightarrow \mathbb{R}^{r \times r}$, $G_{\tau} \in \mathbb{R}^{r \times R}$, $M_{\tau} : \mathbb{R}^{\kappa} \rightarrow \mathbb{R}^r$ defined as*

$$\begin{aligned} \mathcal{Q}_{\tau} &= \frac{w_{\tau}^{\top} w_{\tau}}{d}, & Q_{\tau}(c) &= \frac{w_{\tau}^{\top} \Sigma(c) w_{\tau}}{d}, \\ G_{\tau} &= \frac{w_{\tau}^{\top} E}{\sqrt{d}}, & M_{\tau}(c) &= \frac{w_{\tau}^{\top} \mu(c)}{\sqrt{d}}, \end{aligned} \quad (9)$$

asymptotically converge to the solutions at time $\vartheta = \tau$ of the system of coupled, finite-dimensional, deterministic ODEs

$$\begin{aligned} \frac{d}{d\vartheta} \mathcal{Q}_{\vartheta} &= F_{\mathcal{Q}}(\mathcal{O}_{\vartheta}), & \frac{d}{d\vartheta} Q_{\vartheta} &= F_Q(\mathcal{O}_{\vartheta}) \\ \frac{d}{d\vartheta} G_{\vartheta} &= F_G(\mathcal{O}_{\vartheta}), & \frac{d}{d\vartheta} M_{\vartheta} &= F_M(\mathcal{O}_{\vartheta}) \end{aligned} \quad (10)$$

using the shorthand $\mathcal{O}_{\vartheta} = (\mathcal{Q}_{\vartheta}, Q_{\vartheta}, G_{\vartheta}, M_{\vartheta}, b_{\vartheta})$. The expression for the update functions $F_{\mathcal{Q}, Q, G, M}$ is expounded in Appendix A. The initialization is given by (9) replacing w_{τ} by w_0 . Finally, the value of the skip connection b_{τ} after training from an initialization b_0 is given by the compact closed-form expression

$$b_{\tau} = \frac{\Lambda \mathbb{E}_t[\beta_t]}{\Lambda \mathbb{E}_t[\beta_t^2] + \mathbb{E}_t[\alpha_t^2]} \left[1 - e^{-(\Lambda \mathbb{E}_t[\beta_t^2] + \mathbb{E}_t[\alpha_t^2])\tau} \right] + b_0 e^{-(\Lambda \mathbb{E}_t[\beta_t^2] + \mathbb{E}_t[\alpha_t^2])\tau}, \quad (11)$$

where we denoted Λ the average covariance eigenvalue

$$\Lambda = \int d\pi(c) \int d\nu_c(\omega) \omega. \quad (12)$$

The derivation of Result 2.1, which we detail in Appendix A, follows the ideas of the seminal work of [50, 51], and is very close in spirit to the analysis of [45] for a related model, in the context of data reconstruction. It leverages the observation that in the high-dimensional limit, the SGD steps (5) self-average, and can be captured by a set of deterministic differential equations (10). These ODEs bear over a finite set of low-dimensional summary statistics $\mathcal{Q}, Q, G, M, P, T$ which subsume various geometric characteristics of the weight matrix w_{τ} . Result 2.1 thus importantly subsumes the stochastic, high-dimensional SGD training dynamics (5) in terms of deterministic and low-dimensional processes (10).

2.2 Analysis of the transport

We are now in a position to leverage the summary statistics $\mathcal{Q}_{\tau}, Q_{\tau}, \Theta_{\tau}, M_{\tau}, P, T$ characterized in Result 2.1 –which capture key geometric statistics of the weights w_{τ} of the DAE after training– to analyze the generative SDE (1). A crucial observation is that the SDE (1) is only non-linear in the r -dimensional subspace $\mathcal{W}_{\tau} = \text{span}(w_{\tau}^i)_{i=1}^r$ spanned by the columns of the weight matrix w_{τ} , and is on the other hand linear in the $d - r$ dimensional orthogonal subspace $\mathcal{W}_{\tau}^{\perp}$. The generative dynamics (1) of a sample X_t can accordingly be compactly described by the linear evolution of $Y_t = \Pi_{\mathcal{W}_{\tau}}^{\top} X_t$ (where we denoted $\Pi_{\mathcal{W}_{\tau}}$ the projection in $\mathcal{W}_{\tau}^{\perp}$), and the more complicated but finite-dimensional non-linear evolution of $Z_t = w_{\tau}^{\top} X_t / \sqrt{d}$. This statement is formalized in the following result:

Result 2.2. (generative dynamics) *Let X_t be a stochastic process obeying the generative SDE (1) from an initialization $X_0 \sim \mathcal{N}(0, \mathbb{I}_d)$, and denote $Y_t = \Pi_{\mathcal{W}_{\tau}}^{\top} X_t$ and $Z_t = w_{\tau}^{\top} X_t / \sqrt{d}$. Further define the shorthands*

$$\begin{aligned} \Gamma_t &= \dot{\beta}_t - \frac{\dot{\alpha}_t}{\alpha_t} \beta_t + \epsilon_t \frac{\beta_t}{\alpha_t^2}, & \Delta_t^{\tau} &= b_{\tau} \Gamma_t + \frac{\dot{\alpha}_t}{\alpha_t} - \frac{\epsilon_t}{\alpha_t^2}, \end{aligned} \quad (13)$$

which depend on the schedule functions α, β, ϵ and on the skip connection strength after training b_τ . Then Z_t obeys the low-dimensional SDE

$$\frac{d}{dt}Z_t = \Delta_t^\tau Z_t + \Gamma_t Q_\tau \sigma(Z_t) + \sqrt{2\epsilon_t} Q_\tau^{1/2} dB_t, \quad (14)$$

from an initial condition $Z_0 \sim \mathcal{N}(0, Q_\tau)$, with B a r -dimensional Wiener process. On the other hand, Y_t is independently Gaussian-distributed as

$$Y_t \sim \mathcal{N} \left(0_{\mathcal{W}_\tau^\perp}, e^{2 \int_0^t ds \Delta_s^\tau} \left[1 + 2 \int_0^t e^{-2 \int_0^s dh \Delta_h^\tau} \epsilon_s ds \right] \Pi_{\mathcal{W}_\tau^\perp} \right). \quad (15)$$

The SDE (14) and equation (15) fully describe the law of X_t in terms of only low-dimensional quantities.

We have thus reached a full asymptotic characterization of the evolution of a sample X_t transported by the SDE (1). Qualitatively, the density $\hat{\rho}_\tau(t)$ of X_t is shaped in \mathcal{W}_τ by the action of the DAE network (second term in (14)), which acts as a drift term, while its scale is controlled by the contraction/expansion term Δ_t^τ (first term in (14)), in which the skip connection b_τ intervenes. In \mathcal{W}_τ^\perp , $\hat{\rho}_\tau(t)$ simply remains isotropic and Gaussian, with a time-varying variance succinctly given by (15). This qualitative picture sheds light on the bias of the DAE-parametrized generative model (4). The weights w of the architecture identify and learn important features in the dataset, allowing the model to implement at sampling time a non-trivial transport (14) in the corresponding space \mathcal{W}_τ to approximate the target density. In the orthogonal subspace \mathcal{W}_τ^\perp on the other hand, it is only able to rather crudely approximate the target by an isotropic Gaussian distribution (15), leveraging its skip connection b to adjust the variance thereof.

2.3 Projected density

Result 2.2 completely characterizes the distribution of X_t , allowing to finally reach the desired characterization, namely that of the distribution of the projection $E^\top X_t$ of the generated sample X_t in the reference space \mathcal{E} . We state this characterization in the following result.

Corollary 2.3. (Projected generated density) *The law of the projection $E^\top X_t$ of a sample X_t in the space of interest \mathcal{E} is given by*

$$E^\top X_t \stackrel{d}{=} G_\tau^\top Q_\tau^+ Z_t + \mathcal{N} \left(0_R, e^{2 \int_0^t ds \Delta_s^\tau} \left[1 + 2 \int_0^t e^{-2 \int_0^s dh \Delta_h^\tau} \epsilon_s ds \right] \left(\mathbb{I}_R - G_\tau^\top Q_\tau^+ G_\tau \right) \right), \quad (16)$$

where the law of Z_t is characterized in Result 2.2 by the SDE (14), and the summary statistics Q_τ, G_τ are characterized in Result 2.1. Q_τ^+ denotes the Moore-Penrose pseudo-inverse of Q_τ .

Corollary 2.3 allows to transfer the characterization of Result 2.2, set in a training time dependent space \mathcal{W}_τ , in a fixed, τ -independent subspace \mathcal{E} . Let us remind that the choice of \mathcal{E} is made by the statistician. To give more concrete examples, in the following, when considering Gaussian mixture targets, a natural choice for \mathcal{E} is the space spanned by the cluster centroids. When dealing with unimodal targets with non-trivial covariance, we will choose the space spanned by the principal components.

3 Evolution of the generated density over training time

The theoretical characterizations of Results 2.1, 2.2 and 2.3 afford a complete characterization of low-dimensional projections of the generated density $\hat{\rho}_\tau$ as a function of the network architecture and training time τ . They thereby provide a window to elucidate how the DAE architecture shapes the generated density, and how this bias evolves over training. In the next paragraphs, we discuss these questions in the context of two examples, for a Gaussian mixture density and a real data distribution.

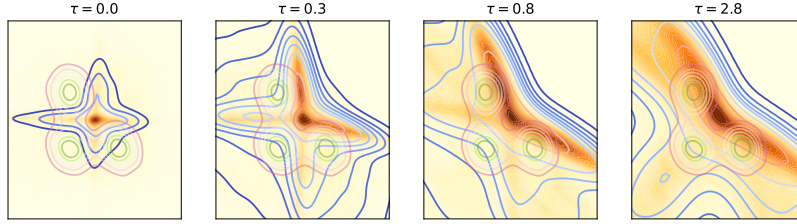


Figure 1: Evolution of the projected density $\Pi_{\mathcal{E}}\hat{\rho}_{\tau}$ generated by a DAE (4) with $r = 4$ hidden units and $\sigma = \text{ReLU}$ activation, trained on a trimodal Gaussian mixture, with $\eta = 0.2, \lambda = 1.5, \epsilon_t = 0, \alpha_t = 1 - t, \beta_t = t, \mathcal{G} = \{0.7\}$, from a warm start. The generative SDE (7) was run up to $t = 0.98$, and the subspace \mathcal{E} is spanned by the centroids of the target density. Different panels correspond to different training times τ . Blue contours: contour levels of the theoretical prediction of Corollary 2.3 for the density $\Pi_{\mathcal{E}}\hat{\rho}_{\tau}$. Colormap: numerical experiments in large but finite dimension $d = 1000$. Green contours: contour levels of the target density ρ . Over training time, the four branches of the generated density rotate to align with the clusters of the target density, with two branches merging in the process.

Example 1 – Gaussian mixture We give as a first example the case of a Gaussian mixture target density ρ with 3 isotropic modes. We consider a generative model parametrized by a DAE (4) with $r = 4$ hidden units and ReLU activation. Fig. 1 illustrates, for different training times τ , the generated density $\hat{\rho}_{\tau}$ projected in the space \mathcal{E} spanned by the cluster centroids of the target density. A comparison between the theoretical predictions (blue contour levels) and numerical experiments in large but finite dimension $d = 1000$ (orange colormap) reveals a good agreement. Interestingly, the modes of the generated density $\hat{\rho}_{\tau}$ rotate over training time to align with the modes of the target density ρ , with two modes merging in the process. The resulting density $\hat{\rho}_{\tau}$ at large training time τ exhibits a similar geometry to the target density ρ , without however perfectly reproducing it – a sign of the architectural bias due to the limited expressivity of the model (4), which cannot perfectly generate the target distribution.

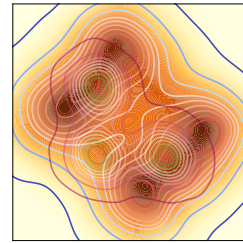


Figure 2: Density $\Pi_{\mathcal{E}}\hat{\rho}_{\tau}$ generated by a DAE (4) with $r = 2$ hidden units and $\sigma = \tanh$ activation, trained on a trimodal Gaussian mixture, with $\eta = 0.2, \lambda = 1.5, \epsilon_t = 0, \alpha_t = 1 - t, \beta_t = t, \mathcal{G} = \{1/2\}, \tau = 2.8$. The generative SDE (7) was run up to $t = 0.98$, and the subspace \mathcal{E} is spanned by the centroids of the target density. Blue contours: contour levels of the theoretical prediction of Corollary 2.3 for the density $\Pi_{\mathcal{E}}\hat{\rho}_{\tau}$. Colormap: numerical experiments in large but finite dimension $d = 1000$. Green contours: contour levels of the target density ρ .

Perhaps unsurprisingly, this bias furthermore strongly depends on the architecture of the DAE. Fig. 2 represents the density generated by a DAE with $r = 2$ hidden units and \tanh activation, for the same target density ρ , with all parameters otherwise unchanged, revealing a very different geometry compared to the ReLU network. In particular, the model fails to generate a trimodal density, with four modes emerging instead. This instance of architectural bias can be easily rationalized. Observe indeed that from equation (14) of Result (2.2), for odd activations such as $\sigma = \tanh$, the transport process is equivariant with respect to the transformation $X \rightarrow -X$. In other words, the generated density $\hat{\rho}_{\tau}$ then necessarily exhibits a symmetry with respect to inversions around the origin –thus forbidding the existence of an odd number of modes. This provides a particularly simple yet telling example of how the choice of architecture can strongly constrain the geometry of the generated densities.

Example 2– MNIST The adaptation of the generated density to the geometry of the target density over training time can also be observed for more realistic distributions. In Fig. 3, a DAE-parametrized generative model with $r = 2$ hidden units and $\sigma = \tanh$ activation is trained to generate a Gaussian distribution with covariance matching that of MNIST sevens [31]. The generated probability $\hat{\rho}_{\tau}$ is represented in the principal two-dimensional eigenspace \mathcal{E} of the MNIST sevens distribution. In a similar fashion to the first example, the generated density progressively adjusts to the shape of the target density (green and purple contours) over training times, first stretching in one direction into a bimodal density ($0 \lesssim \tau \lesssim 1.5$), with each mode being subsequently elongated ($\tau \gtrsim 1.8$), approaching the variance of the target in the secondary direction. This sequential emergence of directions of variance in the generated density has very visual consequences at the level of the

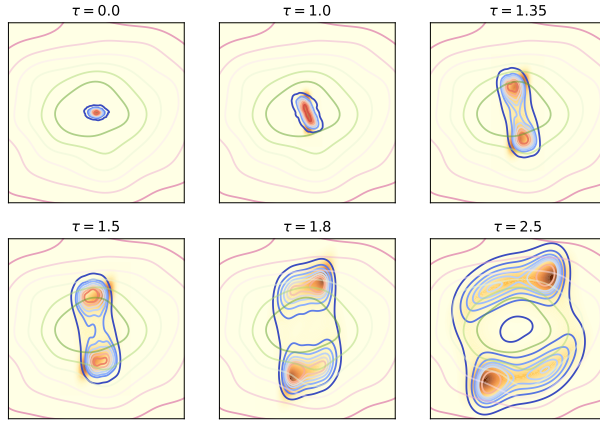


Figure 3: Evolution of the density $\Pi_{\mathcal{E}} \hat{\rho}_{\tau}$ generated by a DAE (4) with $r = 2$ hidden units and $\sigma = \tanh$ activation, trained on a Gaussian density with the MNIST sevens covariance, with $\eta = 0.2$, $\lambda = .784$, $\epsilon_t = 0$, $\alpha_t = 1 - t$, $\beta_t = t$, $\mathcal{G} = \{1/2\}$. The generative SDE (7) was run up to $t = 0.98$, and the subspace \mathcal{E} is spanned by principal components of the target density. Different panels correspond to different training times τ . Blue contours: contour levels of the theoretical prediction of Corollary 2.3 for the density $\hat{\rho}_{\tau}$. Colormap: numerical experiments in large but finite dimension $d = 1000$. Green contours: contour levels of the target density ρ . The generated density is sequentially elongated along the principal components of the target density.

generated images. Fig. 4 shows samples from the generated density $\hat{\rho}_{\tau}$ for varying training times τ , transported from a common base sample X_0 . For $0 \lesssim \tau \lesssim 1.5$, the generated image gains more resolution and becomes less noisy, as the first principal direction is learnt. After $\tau \approx 1.8$, idiosyncratic features – such as the horizontal bar of the seven – emerge, as a second direction is learnt, signaling increased diversity. Interestingly, in the subspace \mathcal{E} , the model is thus approximating a *unimodal* target distribution by a multimodal mixture density. This bias towards multimodal densities can again be traced back to the architecture of the model, and understood from (14) of Result 2.2. Indeed, the drift term $\sigma(Z)$ points towards opposite directions for Z and $-Z$, thereby tending to cleave the distribution into distinct modes, and separating the latter over sampling time t .

Lastly, observe that the modes of the generated density $\hat{\rho}_{\tau}$ display significantly reduced variance in comparison to the target ρ . This dramatic reduction in variance betrays a detrimental bias in the model, which we more extensively explore in the next and last section.

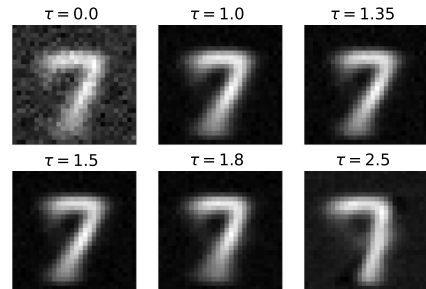


Figure 4: Samples from the generated density $\hat{\rho}_{\tau}$, for a Gaussian target density with covariance matching that of MNIST sevens, from the same initialization X_0 of the generative SDE (7), as a function of the training time τ . The setting is the same as that of Fig. 3. The generated image first shows an enhancement in resolution; additional features (such as the horizontal bar of the seven) emerge subsequently.

4 Failure modes: mode(l) collapse

Mode collapse– The loss of variance in the modes of the generated density $\hat{\rho}_{\tau}$ when learning from the MNIST target distribution (Fig. 3) is reminiscent of the *mode collapse* phenomenon most commonly observed in the context of generative adversarial networks [25] and score-based models [19]. Mode collapse entails a loss in diversity in the generated images. In the present case, mode collapse is again an artifact of the architecture. To see this, first observe that the skip connection b_{τ} of the DAE model (4) contributes to increase the variance of the generated density $\hat{\rho}_{\tau}$, as it intervenes in the linear dilatation term Δ_t^{τ} (13) of the generative transport (14), see Result 2.2. In words, the stronger the strength b_{τ} of the skip connection, the more spread is the resulting generated density. However, note from (11) that the skip connection b_{τ} becomes of the same order as the average eigenvalue Λ at large training times τ . For real data distributions which tend

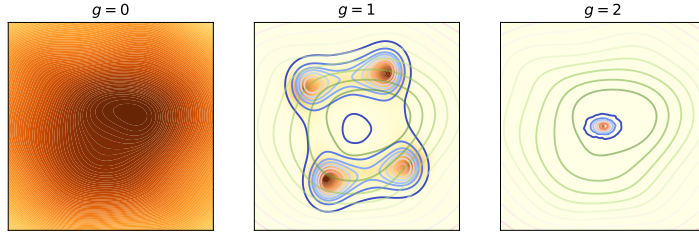


Figure 5: **(left)** Target density ρ corresponding to a Gaussian density equipped with the covariance of the distribution of MNIST sevens **(middle)** generated density $\Pi_{\mathcal{E}} \hat{\rho}_{\tau}^{(1)}$ **(right)** second generation density $\Pi_{\mathcal{E}} \hat{\rho}_{\tau}^{(2)}$ obtained by training the generative model (4) on the synthetic distribution $\hat{\rho}_{\tau}^{(1)}$. Blue contours: contour levels of the theoretical prediction of Corollary 2.3. Colormap: numerical experiments in large but finite dimension $d = 1000$. Green contours: contour levels of the target density ρ . At each successive generations, the same model specifications $\tau = 2.8, r = 2, \sigma = \tanh, \eta = 0.2, \lambda = .784, \epsilon_t = 0, \alpha_t = 1 - t, \beta_t = t, \mathcal{G} = \{1/2\}$ were employed. The generative SDEs (7) were run up to $t = 0.98$ at reach generation. Finally, the subspace \mathcal{E} is spanned by principal components of the target density.

to have a small number of large eigenvalues, and a large tail of small eigenvalues, Λ is typically small, implying in turn a small b_{τ} and small variance for the modes of $\hat{\rho}_{\tau}$. Mode collapse causes a significant mismatch between the generated distribution $\hat{\rho}_{\tau}$ and the target distribution ρ .

Model collapse– This mismatch can be further aggravated when the biased synthetic data thus generated is *re-used* to train another generative model, with successive generations of generated densities $\hat{\rho}_{\tau_1}^{(1)}, \hat{\rho}_{\tau_2}^{(2)}, \dots$ becoming increasingly biased. This rapid degradation is highly reminiscent of the *model collapse* phenomenon described in [55], and can be opportunely also analyzed in the present theoretical framework. To see this, observe that training the generation $g + 1$ model on data produced by the generation g model corresponds to using the density $\hat{\rho}_{\tau_g}^{(g)}$ generated by the latter as a target distribution. Furthermore, this target distribution still falls in the scope of applicability of Results 2.1, 2.2 and 2.3, as at each generation $\hat{\rho}_{\tau_g}^{(g)}$ remains of the form (8). This observation is formalized in the following remark.

Remark 4.1. (Successive generated densities) At each generation, $\hat{\rho}_{\tau_g}^{(g)}$ is again of the form (8), with $\kappa = r, \mu(c) = c$ and

$$\begin{aligned} \pi &= \Pi_{\mathcal{W}_{\tau_g}^{(g)}} \hat{\rho}_{\tau_g}^{(g)}, \\ \Sigma(c) &= e^{2 \int_0^t ds \Delta_s^{\tau_g}} \left[1 + 2 \int_0^t e^{-2 \int_0^s dh \Delta_h^{\tau_g}} \epsilon_s ds \right] \Pi_{\mathcal{W}_{\tau_g}^{(g)}}^{\perp}. \end{aligned} \quad (17)$$

In (17), $\Pi_{\mathcal{W}_{\tau_g}^{(g)}} \hat{\rho}_{\tau_g}^{(g)}, \Delta_s^{\tau_g}$ are given by Results 2.1, 2.2 and 2.3 evaluated for a target density $\hat{\rho}_{\tau_{g-1}}^{(g-1)}$. We remind that $\mathcal{W}_{\tau_g}^{(g)}$ denotes the space spanned by the columns of the trained weights of the generation g model.

In words, Remark 4.1 ensures that one can apply Results 2.1, 2.2 and 2.3 to iteratively reach a characterization of $\hat{\rho}_{\tau_{g+1}}^{(g+1)}$ from that of $\hat{\rho}_{\tau_g}^{(g)}$. Fig. 5 illustrates the first two generations of synthetic distributions $\hat{\rho}_{\tau_1}^{(1)}, \hat{\rho}_{\tau_2}^{(2)}$, when the initial target distribution ρ is given by the same Gaussian approximation of MNIST sevens considered in Figs. 3 and 4. The mode collapse phenomenon described in the previous subsection, and apparent at generation $g = 1$, gets aggravated upon re-training. As a result, the density $\hat{\rho}_{\tau_2}^{(2)}$ generated at $g = 2$ exhibits smaller even variance, and is devoid of meaningful structure.

Conclusions

In this manuscript, we explored the role of the architecture of a diffusion or flow-based generative model in shaping the distribution of generated samples. Considering a model parametrized by a shallow DAE, in the limit of high dimensions, we provided a tight characterization of low-dimensional projections of the generated density. Our results, which also describe tasks with realistically structured target densities, capture how the architectural bias can lead to mode collapse, and ultimately model collapse if the synthetic data is re-used for training.

Limitations— Following a rich stream of previous works [16, 41, 12, 10], we have focused in this work on the class of DAE architectures. Naturally, the bias induced by U-net architectures, equipped with sub/up-sampling layers, could differ [40, 27, 29]. We believe that extending the present sharp analysis to broader classes of architectures is an important future research direction.

Acknowledgements

The authors would like to thank Michael Albergo, Binxu Wang, Sabarish Sainathan, Lenka Zdeborová, and Emanuele Troiani for insightful discussions. HC acknowledges support from the Center of Mathematical Sciences and Applications (CMSA) of Harvard University. CP is supported by NSF Award DMS-2134157, NSF CAREER Award IIS-2239780, and a Sloan Research Fellowship. YML is supported by the Harvard FAS Dean’s Fund for Promising Scholarship, and by a Harvard College Professorship. This work has been made possible in part by a gift from the Chan Zuckerberg Initiative Foundation to establish the Kempner Institute for the Study of Natural and Artificial Intelligence.

References

- [1] Beatrice Achilli, Enrico Ventura, Gianluigi Silvestri, Bao Pham, Gabriel Raya, Dmitry Krotov, Carlo Lucibello, and Luca Ambrogioni. Losing dimensions: Geometric memorization in generative diffusion. *arXiv preprint arXiv:2410.08727*, 2024.
- [2] Michael S Albergo, Nicholas M Boffi, and Eric Vanden-Eijnden. Stochastic interpolants: A unifying framework for flows and diffusions. *arXiv preprint arXiv:2303.08797*, 2023.
- [3] Michael S Albergo and Eric Vanden-Eijnden. Building normalizing flows with stochastic interpolants. *arXiv preprint arXiv:2209.15571*, 2022.
- [4] Iskander Azangulov, George Deligiannidis, and Judith Rousseau. Convergence of diffusion models under the manifold hypothesis in high-dimensions. *arXiv preprint arXiv:2409.18804*, 2024.
- [5] Joe Benton, VD Bortoli, Arnaud Doucet, and George Deligiannidis. Nearly d-linear convergence bounds for diffusion models via stochastic localization. *OpenReview*, 2024.
- [6] Joe Benton, George Deligiannidis, and Arnaud Doucet. Error bounds for flow matching methods. *arXiv preprint arXiv:2305.16860*, 2023.
- [7] Giulio Biroli, Tony Bonnaire, Valentin De Bortoli, and Marc Mézard. Dynamical regimes of diffusion models. *Nature Communications*, 15(1):9957, 2024.
- [8] Giulio Biroli and Marc Mézard. Generative diffusion in very large dimensions. *Journal of Statistical Mechanics: Theory and Experiment*, 2023(9):093402, 2023.
- [9] Adam Block, Youssef Mroueh, and Alexander Rakhlin. Generative modeling with denoising auto-encoders and langevin sampling. *arXiv preprint arXiv:2002.00107*, 2020.
- [10] Nicholas M Boffi, Arthur Jacot, Stephen Tu, and Ingvar Ziemann. Shallow diffusion networks provably learn hidden low-dimensional structure. *arXiv preprint arXiv:2410.11275*, 2024.
- [11] Hongrui Chen, Holden Lee, and Jianfeng Lu. Improved analysis of score-based generative modeling: User-friendly bounds under minimal smoothness assumptions. In *International Conference on Machine Learning*, pages 4735–4763. PMLR, 2023.
- [12] Minshuo Chen, Kaixuan Huang, Tuo Zhao, and Mengdi Wang. Score approximation, estimation and distribution recovery of diffusion models on low-dimensional data. In *International Conference on Machine Learning*, pages 4672–4712. PMLR, 2023.
- [13] Sitan Chen, Sinho Chewi, Holden Lee, Yuanzhi Li, Jianfeng Lu, and Adil Salim. The probability flow ode is provably fast. *Advances in Neural Information Processing Systems*, 36, 2024.
- [14] Sitan Chen, Sinho Chewi, Jerry Li, Yuanzhi Li, Adil Salim, and Anru R Zhang. Sampling is as easy as learning the score: theory for diffusion models with minimal data assumptions. *arXiv preprint arXiv:2209.11215*, 2022.

- [15] Sitan Chen, Vasilis Kontonis, and Kulin Shah. Learning general gaussian mixtures with efficient score matching. *arXiv preprint arXiv:2404.18893*, 2024.
- [16] Hugo Cui, Florent Krzakala, Eric Vanden-Eijnden, and Lenka Zdeborová. Analysis of learning a flow-based generative model from limited sample complexity. *arXiv preprint arXiv:2310.03575*, 2023.
- [17] Hugo Cui and Lenka Zdeborová. High-dimensional asymptotics of denoising autoencoders. *Advances in Neural Information Processing Systems*, 36:11850–11890, 2023.
- [18] Valentin De Bortoli. Convergence of denoising diffusion models under the manifold hypothesis. *arXiv preprint arXiv:2208.05314*, 2022.
- [19] Jacob Deasy, Nikola Simidjievski, and Pietro Liò. Heavy-tailed denoising score matching. *arXiv preprint arXiv:2112.09788*, 2021.
- [20] Zehao Dou, Subhodh Kotekal, Zhehao Xu, and Harrison H Zhou. From optimal score matching to optimal sampling. *arXiv preprint arXiv:2409.07032*, 2024.
- [21] Weiguo Gao and Ming Li. How do flow matching models memorize and generalize in sample data subspaces? *arXiv preprint arXiv:2410.23594*, 2024.
- [22] Khashayar Gatmiry, Jonathan Kelner, and Holden Lee. Learning mixtures of gaussians using diffusion models. *arXiv preprint arXiv:2404.18869*, 2024.
- [23] Davide Ghio, Yatin Dandi, Florent Krzakala, and Lenka Zdeborová. Sampling with flows, diffusion, and autoregressive neural networks from a spin-glass perspective. *Proceedings of the National Academy of Sciences*, 121(27):e2311810121, 2024.
- [24] Sebastian Goldt, Marc Mézard, Florent Krzakala, and Lenka Zdeborová. Modeling the influence of data structure on learning in neural networks: The hidden manifold model. *Physical Review X*, 10(4):041044, 2020.
- [25] Ian Goodfellow, Jean Pouget-Abadie, Mehdi Mirza, Bing Xu, David Warde-Farley, Sherjil Ozair, Aaron Courville, and Yoshua Bengio. Generative adversarial nets. *Advances in neural information processing systems*, 27, 2014.
- [26] Jonathan Ho, Ajay Jain, and Pieter Abbeel. Denoising diffusion probabilistic models. *Advances in neural information processing systems*, 33:6840–6851, 2020.
- [27] Zahra Kadkhodaie, Florentin Guth, Eero P Simoncelli, and Stéphane Mallat. Generalization in diffusion models arises from geometry-adaptive harmonic representation. *arXiv preprint arXiv:2310.02557*, 2023.
- [28] Zahra Kadkhodaie and Eero P Simoncelli. Solving linear inverse problems using the prior implicit in a denoiser. *arXiv preprint arXiv:2007.13640*, 2020.
- [29] Mason Kamb and Surya Ganguli. An analytic theory of creativity in convolutional diffusion models. *arXiv preprint arXiv:2412.20292*, 2024.
- [30] Frederic Koehler, Alexander Heckett, and Andrej Risteski. Statistical efficiency of score matching: The view from isoperimetry. *arXiv preprint arXiv:2210.00726*, 2022.
- [31] Yann LeCun, Léon Bottou, Yoshua Bengio, and Patrick Haffner. Gradient-based learning applied to document recognition. *Proceedings of the IEEE*, 86(11):2278–2324, 1998.
- [32] Holden Lee, Jianfeng Lu, and Yixin Tan. Convergence for score-based generative modeling with polynomial complexity. *Advances in Neural Information Processing Systems*, 35:22870–22882, 2022.
- [33] Holden Lee, Jianfeng Lu, and Yixin Tan. Convergence of score-based generative modeling for general data distributions. In *International Conference on Algorithmic Learning Theory*, pages 946–985. PMLR, 2023.
- [34] Gen Li, Yuting Wei, Yuxin Chen, and Yuejie Chi. Towards faster non-asymptotic convergence for diffusion-based generative models. *arXiv preprint arXiv:2306.09251*, 2023.
- [35] Gen Li and Yuling Yan. Adapting to unknown low-dimensional structures in score-based diffusion models. *arXiv preprint arXiv:2405.14861*, 2024.

- [36] Marvin Li and Sitan Chen. Critical windows: non-asymptotic theory for feature emergence in diffusion models. *arXiv preprint arXiv:2403.01633*, 2024.
- [37] Xiang Li, Yixiang Dai, and Qing Qu. Understanding generalizability of diffusion models requires rethinking the hidden gaussian structure. *arXiv preprint arXiv:2410.24060*, 2024.
- [38] Yaron Lipman, Ricky TQ Chen, Heli Ben-Hamu, Maximilian Nickel, and Matt Le. Flow matching for generative modeling. *arXiv preprint arXiv:2210.02747*, 2022.
- [39] Xingchao Liu, Chengyue Gong, and Qiang Liu. Flow straight and fast: Learning to generate and transfer data with rectified flow. *arXiv preprint arXiv:2209.03003*, 2022.
- [40] Song Mei. U-nets as belief propagation: Efficient classification, denoising, and diffusion in generative hierarchical models. *arXiv preprint arXiv:2404.18444*, 2024.
- [41] Kazusato Oko, Shunta Akiyama, and Taiji Suzuki. Diffusion models are minimax optimal distribution estimators. In *International Conference on Machine Learning*, pages 26517–26582. PMLR, 2023.
- [42] Jakiw Pidstrigach. Score-based generative models detect manifolds. *Advances in Neural Information Processing Systems*, 35:35852–35865, 2022.
- [43] Arnu Pretorius, Steve Kroon, and Herman Kamper. Learning dynamics of linear denoising autoencoders. In *International Conference on Machine Learning*, pages 4141–4150. PMLR, 2018.
- [44] Aditya Ramesh, Prafulla Dhariwal, Alex Nichol, Casey Chu, and Mark Chen. Hierarchical text-conditional image generation with clip latents. *arXiv preprint arXiv:2204.06125*, 1(2):3, 2022.
- [45] Maria Refinetti and Sebastian Goldt. The dynamics of representation learning in shallow, non-linear autoencoders. In *International Conference on Machine Learning*, pages 18499–18519. PMLR, 2022.
- [46] Maria Refinetti, Sebastian Goldt, Florent Krzakala, and Lenka Zdeborová. Classifying high-dimensional gaussian mixtures: Where kernel methods fail and neural networks succeed. In *International Conference on Machine Learning*, pages 8936–8947. PMLR, 2021.
- [47] Robin Rombach, Andreas Blattmann, Dominik Lorenz, Patrick Esser, and Björn Ommer. High-resolution image synthesis with latent diffusion models. In *Proceedings of the IEEE/CVF conference on computer vision and pattern recognition*, pages 10684–10695, 2022.
- [48] Olaf Ronneberger, Philipp Fischer, and Thomas Brox. U-net: Convolutional networks for biomedical image segmentation. In *Medical image computing and computer-assisted intervention—MICCAI 2015: 18th international conference, Munich, Germany, October 5–9, 2015, proceedings, part III 18*, pages 234–241. Springer, 2015.
- [49] Brendan Leigh Ross, Hamidreza Kamkari, Tongzi Wu, Rasa Hosseinzadeh, Zhaoyan Liu, George Stein, Jesse C Cresswell, and Gabriel Loaiza-Ganem. A geometric framework for understanding memorization in generative models. *arXiv preprint arXiv:2411.00113*, 2024.
- [50] David Saad and Sara A Solla. Exact solution for on-line learning in multilayer neural networks. *Physical Review Letters*, 74(21):4337, 1995.
- [51] David Saad and Sara A Solla. On-line learning in soft committee machines. *Physical Review E*, 52(4):4225, 1995.
- [52] Chitwan Saharia, William Chan, Saurabh Saxena, Lala Li, Jay Whang, Emily L Denton, Kamyar Ghasemipour, Raphael Gontijo Lopes, Burcu Karagol Ayan, Tim Salimans, et al. Photorealistic text-to-image diffusion models with deep language understanding. *Advances in neural information processing systems*, 35:36479–36494, 2022.
- [53] Antonio Sclocchi, Alessandro Favero, Noam Itzhak Levi, and Matthieu Wyart. Probing the latent hierarchical structure of data via diffusion models. *arXiv preprint arXiv:2410.13770*, 2024.
- [54] Antonio Sclocchi, Alessandro Favero, and Matthieu Wyart. A phase transition in diffusion models reveals the hierarchical nature of data. *arXiv preprint arXiv:2402.16991*, 2024.
- [55] Ilia Shumailov, Zakhar Shumaylov, Yiren Zhao, Nicolas Papernot, Ross Anderson, and Yarin Gal. Ai models collapse when trained on recursively generated data. *Nature*, 631(8022):755–759, 2024.

- [56] Bernard W Silverman. *Density estimation for statistics and data analysis*. Routledge, 2018.
- [57] Jascha Sohl-Dickstein, Eric Weiss, Niru Maheswaranathan, and Surya Ganguli. Deep unsupervised learning using nonequilibrium thermodynamics. In *International conference on machine learning*, pages 2256–2265. PMLR, 2015.
- [58] Yang Song and Stefano Ermon. Generative modeling by estimating gradients of the data distribution. *Advances in neural information processing systems*, 32, 2019.
- [59] Yang Song, Jascha Sohl-Dickstein, Diederik P Kingma, Abhishek Kumar, Stefano Ermon, and Ben Poole. Score-based generative modeling through stochastic differential equations. *arXiv preprint arXiv:2011.13456*, 2020.
- [60] Joshua B Tenenbaum, Vin de Silva, and John C Langford. A global geometric framework for nonlinear dimensionality reduction. *science*, 290(5500):2319–2323, 2000.
- [61] Pascal Vincent. A connection between score matching and denoising autoencoders. *Neural computation*, 23(7):1661–1674, 2011.
- [62] Pascal Vincent, Hugo Larochelle, Isabelle Lajoie, Yoshua Bengio, Pierre-Antoine Manzagol, and Léon Bottou. Stacked denoising autoencoders: Learning useful representations in a deep network with a local denoising criterion. *Journal of machine learning research*, 11(12), 2010.
- [63] Pauli Virtanen, Ralf Gommers, Travis E. Oliphant, Matt Haberland, Tyler Reddy, David Cournapeau, Evgeni Burovski, Pearu Peterson, Warren Weckesser, Jonathan Bright, Stéfan J. van der Walt, Matthew Brett, Joshua Wilson, K. Jarrod Millman, Nikolay Mayorov, Andrew R. J. Nelson, Eric Jones, Robert Kern, Eric Larson, C J Carey, İlhan Polat, Yu Feng, Eric W. Moore, Jake VanderPlas, Denis Laxalde, Josef Perktold, Robert Cimrman, Ian Henriksen, E. A. Quintero, Charles R. Harris, Anne M. Archibald, Antônio H. Ribeiro, Fabian Pedregosa, Paul van Mulbregt, and SciPy 1.0 Contributors. SciPy 1.0: Fundamental Algorithms for Scientific Computing in Python. *Nature Methods*, 17:261–272, 2020.
- [64] Binxu Wang and John J Vastola. Diffusion models generate images like painters: an analytical theory of outline first, details later. *arXiv preprint arXiv:2303.02490*, 2023.
- [65] Hanyu Wang, Yujin Han, and Difan Zou. On the discrepancy and connection between memorization and generation in diffusion models. *ICML 2024 Workshop on Foundation Models in the Wild*, 2024.
- [66] Wenhao Wang, Yifan Sun, Zongxin Yang, Zhengdong Hu, Zhentao Tan, and Yi Yang. Replication in visual diffusion models: A survey and outlook. *arXiv preprint arXiv:2408.00001*, 2024.
- [67] Joseph L Watson, David Juergens, Nathaniel R Bennett, Brian L Trippe, Jason Yim, Helen E Eisenach, Woody Ahern, Andrew J Borst, Robert J Ragotte, Lukas F Milles, et al. De novo design of protein structure and function with rfdiffusion. *Nature*, 620(7976):1089–1100, 2023.
- [68] Kilian Q Weinberger and Lawrence K Saul. Unsupervised learning of image manifolds by semidefinite programming. *International journal of computer vision*, 70:77–90, 2006.
- [69] Andre Wibisono, Yihong Wu, and Kaylee Yingxi Yang. Optimal score estimation via empirical bayes smoothing. *arXiv preprint arXiv:2402.07747*, 2024.
- [70] TaeHo Yoon, Joo Young Choi, Sehyun Kwon, and Ernest K Ryu. Diffusion probabilistic models generalize when they fail to memorize. In *ICML 2023 Workshop on Structured Probabilistic Inference & Generative Modeling*, 2023.
- [71] Huijie Zhang, Jinfan Zhou, Yifu Lu, Minzhe Guo, Peng Wang, Liyue Shen, and Qing Qu. The emergence of reproducibility and consistency in diffusion models. In *Forty-first International Conference on Machine Learning*, 2023.
- [72] Kaihong Zhang, Caitlyn H Yin, Feng Liang, and Jingbo Liu. Minimax optimality of score-based diffusion models: Beyond the density lower bound assumptions. *arXiv preprint arXiv:2402.15602*, 2024.

A Derivation of Result 2.1

In this Appendix, we detail the derivation of the tight ODE description (10) of the SGD training dynamics (5), as provided in Result 2.1. We sequentially examine the dynamics for the skip connection b and the weight matrix w .

A.1 SGD dynamics of the skip connection

We first derive a closed-form expression for the evolution of the skip connection strength b (4) over the SGD iterations. We recall that the latter read

$$b_{\mu+1} - b_\mu = -\frac{\eta}{d^2} \mathbb{E}_t \left[-2(1 - b\beta_t)\beta_t \|x_1^\mu\|^2 + 2b\alpha_t^2 \|x_0^\mu\|^2 + O(\sqrt{d}) \right], \quad (18)$$

keeping only leading order terms. Note that $\|x_1^\mu\|^2/d$ (resp. $\|x_0^\mu\|^2/d$) asymptotically concentrate to Λ (resp. 1) in the limit $d \rightarrow \infty$. Therefore, the increment $db = b_{\mu+1} - b_\mu$ self-averages as

$$\frac{d}{2\eta} db = \mathbb{E}_t \left[\beta_t(1 - b\beta_t)\Lambda - b\alpha_t^2 \right]. \quad (19)$$

A.2 SGD dynamics of the weight matrix

A.2.1 SGD update

We now turn to deriving a similar tight asymptotic characterization for the evolution of the weight matrix w (4) under the SGD dynamics. Let us first write explicitly the SGD updates (5). Developing the derivative, and dropping the time index μ for readability, for $1 \leq \gamma \leq r, 1 \leq i \leq d$, the SGD update of the weight matrix reads

$$\begin{aligned} dw_{i\gamma} = & -\frac{2\eta}{d} \sum_{\delta=1}^r \mathbb{E}_t \left[\sigma(\omega_\gamma^t) \sigma(\omega_\delta^t) \right] w_{i\delta} + \frac{2\eta}{\sqrt{d}} \mathbb{E}_t \left[((1 - b\beta_t)x_i^1 - b\alpha_t x_i^0) \sigma(\omega_\gamma^t) \right] \\ & - \frac{2\eta}{\sqrt{d}} \mathbb{E}_t \left[(\alpha_t x_i^0 + \beta_t x_i^1) \sum_{\delta=1}^r \sigma(\omega_\delta^t) \left(\frac{w_\delta^\top w_\gamma}{d} \right) \sigma'(\omega_\gamma^t) \right] \\ & + \frac{2\eta}{\sqrt{d}} \mathbb{E}_t \left[(\alpha_t x_i^0 + \beta_t x_i^1) ((1 - b\beta_t)\lambda_\gamma^1 - b\alpha_t \lambda_\gamma^0) \sigma'(\omega_\gamma^t) \right] - \frac{\eta}{d} \lambda w_{i\gamma} \end{aligned} \quad (20)$$

We introduced the shorthands

$$\lambda_\gamma^1 \equiv \frac{w_\gamma^\top x^1}{\sqrt{d}}, \quad \lambda_\gamma^0 \equiv \frac{w_\gamma^\top x^0}{\sqrt{d}}, \quad \omega_\gamma^t = \alpha_t \lambda_\gamma^0 + \beta_t \lambda_\gamma^1. \quad (21)$$

A.2.2 Expected increment

In the likeness of the settings studied by e.g. [50, 51, 45], we expect the dynamics to asymptotically self-average. Let us accordingly evaluate the expectation $\mathbb{E}[dw_{i\gamma}]$ over the running data sample $x_\mu^{1,0}$. This can be compactly rewritten as

$$\mathbb{E}[dw_{i\gamma}] = \mathbb{E}_t \mathbb{E}_c [\mathbb{E}^c dw_{i\gamma}^{t,c}], \quad (22)$$

with the expectation \mathbb{E}_c bearing over the manifold coordinate $c \sim \pi$ (8). Conditional on the manifold coordinate c , the expectation \mathbb{E}^c bears over the Gaussian random variable associated to the c -indexed cluster in (8), distributed as $\mathcal{N}(\mu(c), \Sigma(c))$. We remind the reader that the covariances $\{\Sigma(c)\}_c$ are assumed jointly diagonalizable. Without loss of generality, we place ourselves in the basis in which they are directly diagonal, and denote in the following by ϱ_i^c the

i -th eigenvalue of $\Sigma(c)$. The expected increment then reads

$$\begin{aligned}
\mathbb{E}^c[dw_{i\gamma}^{t,c}] = & -\frac{2\eta}{d} \sum_{\delta=1}^r \underbrace{\mathbb{E}^c \left[\sigma(\omega_\gamma^t) \sigma(\omega_\delta^t) \right]}_{\mathcal{A}_{\gamma\delta}^{t,c}} w_{i\delta} + \frac{2\eta}{\sqrt{d}} (1 - b\beta_t) \underbrace{\mathbb{E}^c \left[x_i^1 \sigma(\omega_\gamma^t) \right]}_{\mathcal{B}_{i\gamma}^{1,t,c}} - \frac{2\eta}{\sqrt{d}} b\alpha_t \underbrace{\mathbb{E}^c \left[x_i^0 \sigma(\omega_\gamma^t) \right]}_{\mathcal{B}_{i\gamma}^{0,t,c}} \\
& - \frac{2\eta}{\sqrt{d}} \alpha_t \sum_{\delta=1}^r \left(\frac{w_\delta^\top w_\gamma}{d} \right) \underbrace{\mathbb{E}^c \left[x_i^0 \sigma(\omega_\delta^t) \sigma'(\omega_\gamma^t) \right]}_{\mathcal{C}_{i\gamma\delta}^{0,t,c}} - \frac{2\eta}{\sqrt{d}} \beta_t \sum_{\delta=1}^r \left(\frac{w_\delta^\top w_\gamma}{d} \right) \underbrace{\mathbb{E}^c \left[x_i^1 \sigma(\omega_\delta^t) \sigma'(\omega_\gamma^t) \right]}_{\mathcal{C}_{i\gamma\delta}^{1,t,c}} \\
& + \frac{2\eta}{\sqrt{d}} \alpha_t (1 - b\beta_t) \underbrace{\mathbb{E}^c \left[x_i^0 \lambda_\gamma^1 \sigma'(\omega_\gamma^t) \right]}_{\mathcal{D}_{i\gamma}^{01,t,c}} - \frac{2\eta}{\sqrt{d}} \alpha_t^2 b \underbrace{\mathbb{E}^c \left[x_i^0 \lambda_\gamma^0 \sigma'(\omega_\gamma^t) \right]}_{\mathcal{D}_{i\gamma}^{00,t,c}} \\
& + \frac{2\eta}{\sqrt{d}} \beta_t (1 - b\beta_t) \underbrace{\mathbb{E}^c \left[x_i^1 \lambda_\gamma^1 \sigma'(\omega_\gamma^t) \right]}_{\mathcal{D}_{i\gamma}^{11,t,c}} - \frac{2\eta}{\sqrt{d}} \alpha_t \beta_t b \underbrace{\mathbb{E}^c \left[x_i^1 \lambda_\gamma^0 \sigma'(\omega_\gamma^t) \right]}_{\mathcal{D}_{i\gamma}^{10,t,c}} - \frac{2\eta}{d} \lambda w_{i\gamma}. \tag{23}
\end{aligned}$$

The various coefficients $\mathcal{A}^{t,c}$, $\mathcal{B}^{t,c}$, $\mathcal{C}^{t,c}$, $\mathcal{D}^{t,c}$ can be evaluated leveraging the fact that the data components $x_i^{1,0}$ are weakly correlated with the local fields ω , $\lambda^{0,1}$, i.e. have $\Theta_d(1/\sqrt{d})$ covariance. Using the expansions for weakly correlated Gaussian variables reported e.g. in [46] (Appendix B.1), we reach

$$\mathcal{A}_{\gamma\delta}^{t,c} = I_{\sigma\sigma}^{t,c}(\gamma, \delta) \tag{24}$$

$$\mathcal{B}_{i\gamma}^{1,t,c} = I_{\sigma'}^{t,c}(\gamma) \mu_i^c + \frac{1}{\sqrt{d}} \frac{\beta_t w_{i\gamma} \varrho_i^c}{\Omega_{\gamma\gamma}^{t,c}} (I_{\sigma\omega}^{t,c}(\gamma, \gamma) - \beta_t M_\gamma^c I_{\sigma'}^{t,c}(\gamma)) \tag{25}$$

$$\mathcal{B}_{i\gamma}^{0,t,c} = \frac{1}{\sqrt{d}} \frac{\alpha_t w_{i\gamma}}{\Omega_{\gamma\gamma}^{t,c}} (I_{\sigma\omega}^{t,c}(\gamma, \gamma) - \beta_t M_\gamma^c I_{\sigma'}^{t,c}(\gamma)) \tag{26}$$

$$\begin{aligned}
\mathcal{C}_{i\gamma\delta}^{0,t,c} = & \frac{1 - \delta_{\gamma\delta}}{\sqrt{d}} \frac{\alpha_t}{\Omega_{\gamma\gamma}^{t,c} \Omega_{\delta\delta}^{t,c} - (\Omega_{\gamma\delta}^{t,c})^2} \left[\left(I_{\sigma'\sigma\omega}^{t,c}(\gamma, \delta, \gamma) - \beta_t M_\gamma^c I_{\sigma'\sigma}^{t,c}(\gamma, \delta) \right) (\Omega_{\delta\delta}^{t,c} w_{i\gamma} - \Omega_{\gamma\delta}^{t,c} w_{i\delta}) \right. \\
& \left. + \left(I_{\sigma'\sigma\omega}^{t,c}(\gamma, \delta, \delta) - \beta_t M_\delta^c I_{\sigma'\sigma}^{t,c}(\gamma, \delta) \right) (\Omega_{\gamma\gamma}^{t,c} w_{i\delta} - \Omega_{\gamma\delta}^{t,c} w_{i\gamma}) \right] \\
& + \frac{\delta_{\gamma\delta}}{\Omega_{\gamma\gamma}^{t,c}} \alpha_t w_{i\gamma} (I_{\sigma'\sigma\omega}^{t,c}(\gamma, \gamma, \gamma) - \beta_t M_\gamma^c I_{\sigma'\sigma}^{t,c}(\gamma, \gamma)) \tag{27}
\end{aligned}$$

$$\mathcal{C}_{i\gamma\delta}^{1,t,c} = I_{\sigma'\sigma}^{t,c}(\gamma, \delta) \mu_i^c + \frac{\beta_t \varrho_i^c}{\alpha_t} \mathcal{C}_{i\gamma\delta}^{0,t,c} \tag{28}$$

$$\mathcal{D}_{i\gamma}^{01,t,c} = \frac{1}{\sqrt{d}} \frac{Q_{\gamma\gamma}^c \alpha_t w_{i\gamma}}{Q_{\gamma\gamma}^c \Omega_{\gamma\gamma}^{t,c} - \beta_t^2 (Q_{\gamma\gamma}^c)^2} \left[I_{\lambda^1 \sigma' \omega}^{t,c}(\gamma, \gamma, \gamma) - \beta_t I_{(\lambda^1)^2 \sigma'}^{t,c}(\gamma, \gamma) \right] \tag{29}$$

$$\mathcal{D}_{i\gamma}^{00,t,c} = \frac{1}{\sqrt{d}} \frac{w_{i\gamma}}{Q_{\gamma\gamma} \Omega_{\gamma\gamma}^{t,c} - \alpha_t^2 (Q_{\gamma\gamma})^2} \left[I_{(\lambda^0)^2 \sigma'}^{t,c}(\gamma, \gamma) (\Omega_{\gamma\gamma}^{t,c} - \alpha_t^2 Q_{\gamma\gamma}) \right] \tag{30}$$

$$\mathcal{D}_{i\gamma}^{10,t,c} = \mu_i^c I_{\lambda^0 \sigma'}^{t,c}(\gamma, \gamma) + \frac{1}{\sqrt{d}} \frac{Q_{\gamma\gamma} \beta_t \varrho_i^c w_{i\gamma}}{Q_{\gamma\gamma} \Omega_{\gamma\gamma}^{t,c} - \alpha_t^2 (Q_{\gamma\gamma})^2} \left[I_{\lambda^0 \sigma' \omega}^{t,c}(\gamma, \gamma, \gamma) - \alpha_t I_{(\lambda^0)^2 \sigma'}^{t,c}(\gamma, \gamma) - M_\gamma^c \beta_t I_{\lambda^0 \sigma'}^{t,c}(\gamma, \gamma) \right] \tag{31}$$

$$\mathcal{D}_{i\gamma}^{11,t,c} = \mu_i^c I_{\lambda^1 \sigma'}^{t,c}(\gamma, \gamma) + \frac{1}{\sqrt{d}} \frac{w_{i\gamma} \varrho_i^c}{Q_{\gamma\gamma}^c \Omega_{\gamma\gamma}^{t,c} - \beta_t^2 (Q_{\gamma\gamma}^c)^2} \left[(I_{(\lambda^1)^2 \sigma'}^{t,c}(\gamma, \gamma) - M_\gamma^c I_{\lambda^1 \sigma'}^{t,c}(\gamma, \gamma)) (\Omega_{\gamma\gamma}^{t,c} - \beta_t^2 Q_{\gamma\gamma}^c) \right]. \tag{32}$$

We introduced the summary statistics

$$M^c = \frac{w^\top \mu(c)}{\sqrt{d}}, \quad Q^c = \frac{w^\top \Sigma(c) w}{d}, \tag{33}$$

$$\mathcal{Q} = \frac{w^\top w}{d}, \quad \Omega^{t,c} = \alpha_t^2 \mathcal{Q} + \beta_t^2 Q^c, \quad T^{ck} = \mu(c)^\top \mu(k) \tag{34}$$

One also needs to introduce the further statistics

$$G = \frac{w^\top E}{\sqrt{d}}, \quad P^c = E^\top \mu(c), \quad (35)$$

where we remind that the columns of $E \in \mathbb{R}^{d \times R}$ constitute an orthonormal basis of the R -dimensional subspace \mathcal{E} in which we aim to characterize the generated density. Finally, we also used the shorthands:

$$I_{\sigma\sigma}^{t,c}(\gamma, \delta) = \mathbb{E}_{\omega_\gamma, \omega_\delta} [\sigma(\omega_\gamma)\sigma(\omega_\delta)], \quad \omega_\gamma, \omega_\delta \sim \mathcal{N}\left(\beta_t M_{(\gamma,\delta)}^c, \Omega_{(\gamma,\delta)}^{t,c}\right) \quad (36)$$

$$I_{\sigma'}^{t,c}(\gamma) = \mathbb{E}_{\omega_\gamma} [\sigma'(\omega_\gamma)], \quad \omega_\gamma \sim \mathcal{N}\left(\beta_t M_\gamma^c, \Omega_{\gamma\gamma}^{t,c}\right) \quad (37)$$

$$I_{\sigma\omega}^{t,c}(\gamma, \delta) = \mathbb{E}_{\omega_\gamma, \omega_\delta} [\sigma(\omega_\gamma)\omega_\delta], \quad \omega_\gamma, \omega_\delta \sim \mathcal{N}\left(\beta_t M_{(\gamma,\delta)}^c, \Omega_{(\gamma,\delta)}^{t,c}\right) \quad (38)$$

$$I_{\sigma'\sigma\omega}^{t,c}(\gamma, \delta, \epsilon) = \mathbb{E}_{\omega_\gamma, \omega_\delta, \omega_\epsilon} [\sigma'(\omega_\gamma)\sigma(\omega_\delta)\omega_\epsilon], \quad \omega_\gamma, \omega_\delta, \omega_\epsilon \sim \mathcal{N}\left(\beta_t M_{(\gamma,\delta,\epsilon)}^c, \Omega_{(\gamma,\delta,\epsilon)}^{t,c}\right) \quad (39)$$

$$I_{\sigma'\sigma}^{t,c}(\gamma, \delta) = \mathbb{E}_{\omega_\gamma, \omega_\delta} [\sigma'(\omega_\gamma)\sigma(\omega_\delta)], \quad \omega_\gamma, \omega_\delta \sim \mathcal{N}\left(\beta_t M_{(\gamma,\delta)}^c, \Omega_{(\gamma,\delta)}^{t,c}\right), \quad (40)$$

and

$$I_{\lambda^1 \sigma'\omega}^{t,c}(\gamma, \delta, \epsilon) = \mathbb{E}_{\lambda_\gamma^1, \omega_\delta, \omega_\epsilon} [\lambda_\gamma^1 \sigma'(\omega_\delta)\omega_\epsilon], \quad \lambda_\gamma^1, \omega_\delta, \omega_\epsilon \sim \mathcal{N}\left(\left(\begin{array}{c} M_\gamma^c \\ \beta_t M_{(\delta,\epsilon)}^c \end{array}\right), \left(\begin{array}{cc} Q_{\gamma\gamma}^c & \beta_t Q_{\gamma,(\delta,\epsilon)}^c \\ \beta_t (Q_{\gamma,(\delta,\epsilon)}^c)^\top & \Omega_{(\delta,\epsilon)}^{t,c} \end{array}\right)\right) \quad (41)$$

$$I_{(\lambda^1)^2 \sigma'}^{t,c}(\gamma, \delta) = \mathbb{E}_{\omega_\gamma, \omega_\delta} [(\lambda_\gamma^1)^2 \sigma'(\omega_\delta)], \quad \lambda_\gamma^1, \omega_\delta \sim \mathcal{N}\left(\left(\begin{array}{c} M_\gamma^c \\ \beta_t M_\delta^c \end{array}\right), \left(\begin{array}{cc} Q_{\gamma\gamma}^c & \beta_t Q_{\gamma,\delta}^c \\ \beta_t (Q_{\gamma,\delta}^c) & \Omega_\delta^{t,c} \end{array}\right)\right) \quad (42)$$

$$I_{\lambda^0 \sigma'\omega}^{t,c}(\gamma, \delta, \epsilon) = \mathbb{E}_{\lambda_\gamma^0, \omega_\delta, \omega_\epsilon} [\lambda_\gamma^0 \sigma'(\omega_\delta)\omega_\epsilon], \quad \lambda_\gamma^0, \omega_\delta, \omega_\epsilon \sim \mathcal{N}\left(\left(\begin{array}{c} 0 \\ \beta_t M_{(\delta,\epsilon)}^c \end{array}\right), \left(\begin{array}{cc} Q_{\gamma\gamma} & \alpha_t Q_{\gamma,(\delta,\epsilon)} \\ \alpha_t (Q_{\gamma,(\delta,\epsilon)})^\top & \Omega_{(\delta,\epsilon)}^{t,c} \end{array}\right)\right) \quad (43)$$

$$I_{(\lambda^0)^2 \sigma'}^{t,c}(\gamma, \delta) = \mathbb{E}_{\omega_\gamma, \omega_\delta} [(\lambda_\gamma^0)^2 \sigma'(\omega_\delta)], \quad \lambda_\gamma^0, \omega_\delta \sim \mathcal{N}\left(\left(\begin{array}{c} 0 \\ \beta_t M_\delta^c \end{array}\right), \left(\begin{array}{cc} Q_{\gamma\gamma} & \alpha_t Q_{\gamma,\delta} \\ \alpha_t (Q_{\gamma,\delta}) & \Omega_\delta^{t,c} \end{array}\right)\right) \quad (44)$$

(45)

A.2.3 Update equation for the summary statistics

The training dynamics of the DAE weights w are thus governed by set of finite-dimensional summary statistics. To close the equations and reach a self-contained characterization, we now turn to deriving the induced dynamics of the summary statistics. To that end, following e.g. [24], it proves convenient to first introduce a new set of summary statistics *densities*. For any $\varrho : \mathbb{R}^\kappa \rightarrow \mathbb{R}$ -denoting a joint sequence of eigenvalues $\{\varrho(c)\}$ -, let us assume the existence of the densities $m, p : \mathbb{R}^\kappa \times \mathcal{F}(\mathbb{R}^\kappa, \mathbb{R}) \rightarrow \mathbb{R}$, $q, g : \times \mathcal{F}(\mathbb{R}^\kappa, \mathbb{R}) \rightarrow \mathbb{R}$ and $\theta : (\mathbb{R}^\kappa)^2 \times \mathcal{F}(\mathbb{R}^\kappa, \mathbb{R}) \rightarrow \mathbb{R}$ so that the summary statistics $M^c, \Omega, Q^c, T, G, P$ (33) can be decomposed as

$$M^c = \int d\varrho m^c(\varrho), \quad (46)$$

$$Q^c = \int d\varrho q(\varrho) \varrho_c, \quad (47)$$

$$\Omega = \int d\varrho q(\varrho), \quad (48)$$

$$T^{ck} = \int d\varrho \theta^{ck}(\varrho), \quad (49)$$

$$G = \int d\varrho g(\varrho), \quad (50)$$

$$P^c = \int d\varrho p^c(\varrho), \quad (51)$$

The following subsections focus on deriving the updates of the summary statistic densities $m(\cdot), q(\cdot), \theta(\cdot), g(\cdot)$ inherited from the SGD dynamics of the weight matrix w (23).

A.2.4 Overlap $m^k(\cdot)$

The expected increment for $m^k(\varrho)$ can also be decomposed as

$$\mathbb{E}[dm^k(\varrho)] = \mathbb{E}_t \mathbb{E}_c \left[\mathbb{E}^c dm_k^{t,c}(\varrho) \right], \quad (52)$$

with

$$\begin{aligned} \frac{d}{2\eta} \mathbb{E}^c [dm_k^{t,c}(\varrho)_\gamma] &= - \sum_{\delta=1}^r I_{\sigma\sigma}^{t,c}(\gamma, \delta) m^k(\varrho)_\delta + (1 - b\beta_t) I_{\sigma}^{t,c}(\gamma) \theta^{ck}(\varrho) \\ &+ \frac{(1 - b\beta_t) \beta_t \varrho_c m^k(\varrho)_\gamma - b\alpha_t^2 m^k(\varrho)_\gamma}{\Omega_{\gamma\gamma}^{t,c}} (I_{\sigma\omega}^{t,c}(\gamma, \gamma) - \beta_t M_\gamma^c I_{\sigma}^{t,c}(\gamma)) \\ &- \sum_{\delta \neq \gamma} \frac{(\alpha_t^2 + \beta_t^2 \varrho_c) \Omega_{\gamma\delta}}{\Omega_{\gamma\gamma}^{t,c} \Omega_{\delta\delta}^{t,c} - (\Omega_{\gamma\delta}^{t,c})^2} \left[(I_{\sigma'\sigma\omega}^{t,c}(\gamma, \delta, \gamma) - \beta_t M_\gamma^c I_{\sigma'\sigma}^{t,c}(\gamma, \delta)) (\Omega_{\delta\delta}^{t,c} m^k(\varrho)_\gamma - \Omega_{\gamma\delta}^{t,c} m^k(\varrho)_\delta) \right. \\ &\quad \left. + (I_{\sigma'\sigma\omega}^{t,c}(\gamma, \delta, \delta) - \beta_t M_\delta^c I_{\sigma'\sigma}^{t,c}(\gamma, \delta)) (\Omega_{\gamma\gamma}^{t,c} m^k(\varrho)_\delta - \Omega_{\gamma\delta}^{t,c} m^k(\varrho)_\gamma) \right] \\ &- \frac{\Omega_{\gamma\gamma} (\alpha_t^2 + \beta_t^2 \varrho_c) m^k(\varrho)_\gamma}{\Omega_{\gamma\gamma}^{t,c}} (I_{\sigma'\sigma\omega}^{t,c}(\gamma, \gamma, \gamma) - \beta_t M_\gamma^c I_{\sigma'\sigma}^{t,c}(\gamma, \gamma)) - \beta_t \sum_{\delta=1}^r \Omega_{\gamma\delta} I_{\sigma'\sigma}^{t,c}(\gamma, \delta) \theta^{ck}(\varrho) \\ &+ \frac{\alpha_t^2 (1 - b\beta_t) Q_{\gamma\gamma}^c m^k(\varrho)_\gamma}{Q_{\gamma\gamma}^c \Omega_{\gamma\gamma}^{t,c} - \beta_t^2 (Q_{\gamma\gamma}^c)^2} \left[I_{\lambda^1 \sigma'\omega}^{t,c}(\gamma, \gamma, \gamma) - \beta_t I_{(\lambda^1)^2 \sigma'}^{t,c}(\gamma, \gamma) \right] \\ &- \frac{\alpha_t^2 b m^k(\varrho)_\gamma}{\Omega_{\gamma\gamma} \Omega_{\gamma\gamma}^{t,c} - \alpha_t^2 (Q_{\gamma\gamma})^2} \left[I_{(\lambda^0)^2 \sigma'}^{t,c}(\gamma, \gamma) (\Omega_{\gamma\gamma}^{t,c} - \alpha_t^2 Q_{\gamma\gamma}) \right] \\ &+ \beta_t (1 - b\beta_t) I_{\lambda^1 \sigma'}^{t,c}(\gamma, \gamma) \theta^{ck}(\varrho) \\ &+ \frac{\beta_t (1 - b\beta_t) \varrho_c m^k(\varrho)_\gamma}{Q_{\gamma\gamma}^c \Omega_{\gamma\gamma}^{t,c} - \beta_t^2 (Q_{\gamma\gamma}^c)^2} \left[(I_{(\lambda^1)^2 \sigma'}^{t,c}(\gamma, \gamma) - M_\gamma^c I_{\lambda^1 \sigma'}^{t,c}(\gamma, \gamma)) (\Omega_{\gamma\gamma}^{t,c} - \beta_t^2 Q_{\gamma\gamma}^c) \right] \\ &- \alpha_t \beta_t b I_{\lambda^0 \sigma'}(\gamma, \gamma) \theta^{ck}(\varrho) \\ &- \frac{\Omega_{\gamma\gamma} b \beta_t \alpha_t^2 \varrho_c m^k(\varrho)_\gamma}{\Omega_{\gamma\gamma} \Omega_{\gamma\gamma}^{t,c} - \alpha_t^2 (Q_{\gamma\gamma})^2} \left[I_{\lambda^0 \sigma'\omega}^{t,c}(\gamma, \gamma, \gamma) - \alpha_t I_{(\lambda^0)^2 \sigma'}^{t,c}(\gamma, \gamma) - M_\gamma^c \beta_t I_{\lambda^0 \sigma'}^{t,c}(\gamma, \gamma) \right] \\ &- \lambda m^k(\varrho)_\gamma \end{aligned} \quad (53)$$

A.2.5 Overlap $g(\cdot)$

The expected SGD for $g(\varrho)$ can be derived along nearly identical lines. By the same token, for $1 \leq i \leq R$, the decomposition

$$\mathbb{E}[dg_i(\varrho)] = \mathbb{E}_t \mathbb{E}_c \left[\mathbb{E}^c dg_i^{t,c}(\varrho) \right] \quad (54)$$

holds with

$$\begin{aligned}
\frac{d}{2\eta}\mathbb{E}^c[dg^{t,c}(\varrho)_\gamma] &= -\sum_{\delta=1}^r I_{\sigma\sigma}^{t,c}(\gamma, \delta)g_i(\varrho)_\delta + (1-b\beta_t)I_{\sigma}^{t,c}(\gamma)p_i^c(\varrho) \\
&+ \frac{(1-b\beta_t)\beta_t\varrho_c g_i(\varrho)_\gamma - b\alpha_t^2 g_i(\varrho)_\gamma}{\Omega_{\gamma\gamma}^{t,c}}(I_{\sigma\omega}^{t,c}(\gamma, \gamma) - \beta_t M_\gamma^c I_{\sigma}^{t,c}(\gamma)) \\
&- \sum_{\delta \neq \gamma} \frac{(\alpha_t^2 + \beta_t^2 \varrho_c)\mathcal{Q}_{\gamma\delta}}{\Omega_{\gamma\gamma}^{t,c}\Omega_{\delta\delta}^{t,c} - (\Omega_{\gamma\delta}^{t,c})^2} \left[(I_{\sigma'\sigma\omega}^{t,c}(\gamma, \delta, \gamma) - \beta_t M_\gamma^c I_{\sigma'\sigma}^{t,c}(\gamma, \delta))(\Omega_{\delta\delta}^{t,c} g_i(\varrho)_\gamma - \Omega_{\gamma\delta}^{t,c} g_i(\varrho)_\delta) \right. \\
&\quad \left. + (I_{\sigma'\sigma\omega}^{t,c}(\gamma, \delta, \delta) - \beta_t M_\delta^c I_{\sigma'\sigma}^{t,c}(\gamma, \delta))(\Omega_{\gamma\gamma}^{t,c} g(\varrho)_\delta - \Omega_{\gamma\delta}^{t,c} g(\varrho)_\gamma) \right] \\
&- \frac{\mathcal{Q}_{\gamma\gamma}(\alpha_t^2 + \beta_t^2 \varrho_c)g_i(\varrho)_\gamma}{\Omega_{\gamma\gamma}^{t,c}}(I_{\sigma'\sigma\omega}^{t,c}(\gamma, \gamma, \gamma) - \beta_t M_\gamma^c I_{\sigma'\sigma}^{t,c}(\gamma, \gamma)) - \beta_t \sum_{\delta=1}^r \mathcal{Q}_{\gamma\delta} I_{\sigma'\sigma}^{t,c}(\gamma, \delta)p_i^c(\varrho) \\
&+ \frac{\alpha_t^2(1-b\beta_t)\mathcal{Q}_{\gamma\gamma}^c g_i(\varrho)_\gamma}{\mathcal{Q}_{\gamma\gamma}^c \Omega_{\gamma\gamma}^{t,c} - \beta_t^2 (\mathcal{Q}_{\gamma\gamma}^c)^2} \left[I_{\lambda^1 \sigma'\omega}^{t,c}(\gamma, \gamma, \gamma) - \beta_t I_{(\lambda^1)^2 \sigma'}^{t,c}(\gamma, \gamma) \right] \\
&- \frac{\alpha_t^2 b g_i(\varrho)_\gamma}{\mathcal{Q}_{\gamma\gamma} \Omega_{\gamma\gamma}^{t,c} - \alpha_t^2 (\mathcal{Q}_{\gamma\gamma})^2} \left[I_{(\lambda^0)^2 \sigma'}^{t,c}(\gamma, \gamma)(\Omega_{\gamma\gamma}^{t,c} - \alpha_t^2 \mathcal{Q}_{\gamma\gamma}) \right] \\
&+ \beta_t(1-b\beta_t)I_{\lambda^1 \sigma'}^{t,c}(\gamma, \gamma)p_i^c(\varrho) \\
&+ \frac{\beta_t(1-b\beta_t)\varrho_c g_i(\varrho)_\gamma}{\mathcal{Q}_{\gamma\gamma}^c \Omega_{\gamma\gamma}^{t,c} - \beta_t^2 (\mathcal{Q}_{\gamma\gamma}^c)^2} \left[(I_{(\lambda^1)^2 \sigma'}^{t,c}(\gamma, \gamma) - M_\gamma^c I_{\lambda^1 \sigma'}^{t,c}(\gamma, \gamma))(\Omega_{\gamma\gamma}^{t,c} - \beta_t^2 \mathcal{Q}_{\gamma\gamma}^c) \right] \\
&- \alpha_t \beta_t b I_{\lambda^0 \sigma'}^{t,c}(\gamma, \gamma)p_i^c(\varrho) \\
&- \frac{\mathcal{Q}_{\gamma\gamma} b \beta_t \alpha_t^2 \varrho_c g_i(\varrho)_\gamma}{\mathcal{Q}_{\gamma\gamma} \Omega_{\gamma\gamma}^{t,c} - \alpha_t^2 (\mathcal{Q}_{\gamma\gamma})^2} \left[I_{\lambda^0 \sigma'\omega}^{t,c}(\gamma, \gamma, \gamma) - \alpha_t I_{(\lambda^0)^2 \sigma'}^{t,c}(\gamma, \gamma) - M_\gamma^c \beta_t I_{\lambda^0 \sigma'}^{t,c}(\gamma, \gamma) \right] \\
&- \lambda g_i(\varrho)_\gamma, \tag{55}
\end{aligned}$$

yielding the increment of $g(\cdot)$ under the SGD dynamics.

A.2.6 Overlap $q(\cdot)$

We now turn to the summary statistic $q(\varrho)$ (33). First note that

$$\begin{aligned}
\mathbb{E}[d\mathcal{Q}] &= \frac{1}{d} \sum_{i=1}^d \mathbb{E}_c \left[w_i \mathbb{E}_t [\mathbb{E}^c dw_i^{t,c}]^\top + \mathbb{E}_t [\mathbb{E}^c dw_i^{t,c}] w_i^\top + \mathbb{E}_{t,t'} [\mathbb{E}^c dw_i^{t,c} (dw_i^{t',c})^\top] \right] \\
&\equiv \mathbb{E}_t \mathbb{E}_c [\mathbb{E}^c d\mathcal{Q}_{(1)}^{t,c}(\varrho)] + \mathbb{E}_{t,t'} \mathbb{E}_c [\mathbb{E}^c d\mathcal{Q}_{(2)}^{t,t',c}(\varrho)]. \tag{56}
\end{aligned}$$

We have separated the linear term and the quadratic term. It follows that the density statistic $q(\cdot)$ can be similarly decomposed as

$$\mathbb{E}[dq(\varrho)] = \mathbb{E}_t \mathbb{E}_c [\mathbb{E}^c dq_{(1)}^{t,c}(\varrho)] + \mathbb{E}_{t,t'} \mathbb{E}_c [\mathbb{E}^c dq_{(2)}^{t,t',c}(\varrho)]. \tag{57}$$

In the following, we sequentially examine the linear and quadratic terms. The expected increment for the linear term $dq_{(1)}^{t,c}(\cdot)$ can be read from (23) as

$$\begin{aligned}
\frac{d}{2\eta} \mathbb{E}^c[(dq_{(1)}^{t,c}(\varrho))_{\gamma\delta}] &= - \sum_{\epsilon=1}^r I_{\sigma\sigma}^{t,c}(\gamma, \epsilon) q(\varrho)_{\delta\epsilon} + (1 - b\beta_t) I_{\sigma}^{t,c}(\gamma) m^c(\varrho)_{\delta} \\
&+ \frac{((1 - b\beta_t)\beta_t \varrho_c - b\alpha_t^2) q(\varrho)_{\gamma\delta}}{\Omega_{\gamma\gamma}^{t,c}} (I_{\sigma\omega}^{t,c}(\gamma, \gamma) - \beta_t M_{\gamma}^c I_{\sigma}^{t,c}(\gamma)) \\
&- \sum_{\epsilon \neq \gamma} \frac{(\alpha_t^2 + \beta_t^2 \varrho_c) \mathcal{Q}_{\epsilon\gamma}}{\Omega_{\gamma\gamma}^{t,c} \Omega_{\epsilon\epsilon}^{t,c} - (\Omega_{\gamma\epsilon}^{t,c})^2} \left[\left(I_{\sigma'\sigma\omega}^{t,c}(\gamma, \epsilon, \gamma) - \beta_t M_{\gamma}^c I_{\sigma'\sigma}^{t,c}(\gamma, \epsilon) \right) (\Omega_{\epsilon\epsilon}^{t,c} q(\varrho)_{\gamma\delta} - \Omega_{\gamma\epsilon}^{t,c} q(\varrho)_{\epsilon\delta}) \right. \\
&\quad \left. + \left(I_{\sigma'\sigma\omega}^{t,c}(\gamma, \epsilon, \epsilon) - \beta_t M_{\epsilon}^c I_{\sigma'\sigma}^{t,c}(\gamma, \epsilon) \right) (\Omega_{\gamma\gamma}^{t,c} q(\varrho)_{\delta\epsilon} - \Omega_{\gamma\epsilon}^{t,c} q(\varrho)_{\gamma\delta}) \right] \\
&- \frac{(\alpha_t^2 + \beta_t^2 \varrho_c) \mathcal{Q}_{\gamma\gamma} q(\varrho)_{\gamma\delta}}{\Omega_{\gamma\gamma}^{t,c}} (I_{\sigma'\sigma\omega}^{t,c}(\gamma, \gamma, \gamma) - \beta_t M_{\gamma}^c I_{\sigma'\sigma}^{t,c}(\gamma, \gamma)) - \beta_t \sum_{\epsilon=1}^r \mathcal{Q}_{\epsilon\gamma} I_{\sigma'\sigma}^{t,c}(\gamma, \epsilon) m^c(\varrho)_{\delta} \\
&+ \frac{Q_{\gamma\gamma}^c \alpha_t^2 (1 - b\beta_t) q(\varrho)_{\gamma\delta}}{Q_{\gamma\gamma}^c \Omega_{\gamma\gamma}^{t,c} - \beta_t^2 (Q_{\gamma\gamma}^c)^2} \left[I_{\lambda^1 \sigma'\omega}^{t,c}(\gamma, \gamma, \gamma) - \beta_t I_{(\lambda^1)^2 \sigma'}^{t,c}(\gamma, \gamma) \right] \\
&- \frac{\alpha_t^2 b q(\varrho)_{\gamma\delta}}{Q_{\gamma\gamma} \Omega_{\gamma\gamma}^{t,c} - \alpha_t^2 (Q_{\gamma\gamma})^2} \left[I_{(\lambda^0)^2 \sigma'}^{t,c}(\gamma, \gamma) (\Omega_{\gamma\gamma}^{t,c} - \alpha_t^2 Q_{\gamma\gamma}) \right] \\
&+ \beta_t (1 - b\beta_t) I_{\lambda^1 \sigma'}^{t,c}(\gamma, \gamma) m^c(\varrho)_{\delta} \\
&+ \frac{\beta_t (1 - b\beta_t) q(\varrho)_{\gamma\delta} \varrho^c}{Q_{\gamma\gamma} \Omega_{\gamma\gamma}^{t,c} - \beta_t^2 (Q_{\gamma\gamma}^c)^2} \left[(I_{(\lambda^1)^2 \sigma'}^{t,c}(\gamma, \gamma) - M_{\gamma}^c I_{\lambda^1 \sigma'}^{t,c}(\gamma, \gamma)) (\Omega_{\gamma\gamma}^{t,c} - \beta_t^2 Q_{\gamma\gamma}^c) \right] \\
&- \alpha_t \beta_t b I_{\lambda^0 \sigma'}^{t,c}(\gamma, \gamma) m^c(\varrho)_{\delta} \\
&- \frac{\alpha_t^2 \beta_t b Q_{\gamma\gamma} \varrho^c q(\varrho)_{\gamma\delta}}{Q_{\gamma\gamma} \Omega_{\gamma\gamma}^{t,c} - \alpha_t^2 (Q_{\gamma\gamma})^2} \left[I_{\lambda^0 \sigma'\omega}^{t,c}(\gamma, \gamma, \gamma) - \alpha_t I_{(\lambda^0)^2 \sigma'}^{t,c}(\gamma, \gamma) - M_{\gamma}^c \beta_t I_{\lambda^0 \sigma'}^{t,c}(\gamma, \gamma) \right] \\
&- \lambda q(\varrho)_{\gamma\delta} \\
&+ (\gamma \leftrightarrow \delta)
\end{aligned} \tag{58}$$

We now turn to the quadratic term $dq_{(2)}^{t,c}(\cdot)$. Keeping only leading order terms,

$$\begin{aligned}
\frac{d}{4\eta^2} \mathbb{E}^c[(dq_{(2)}^{t,c}(\varrho))_{\gamma\delta}] &= \frac{1}{2} \nu(\varrho) I_{\sigma\sigma}^{t,t',c}(\gamma, \delta) \left[(1 - b\beta_t)(1 - b\beta_{t'}) \varrho_c + b^2 \alpha_t \alpha_{t'} \right] \\
&- \nu(\varrho) \sum_{\epsilon=1}^r I_{\sigma\sigma\sigma'}^{t,t',c}(\gamma, \epsilon, \delta) \mathcal{Q}_{\epsilon\delta} [\beta_{t'} (1 - b\beta_t) \varrho_c - b\alpha_t \alpha_{t'}] \\
&+ \nu(\varrho) \left((1 - b\beta_{t'}) I_{\sigma\sigma'\lambda^1}^{t,t',c}(\gamma, \delta, \delta) - b\alpha_{t'} I_{\sigma\sigma'\lambda^0}^{t,t',c}(\gamma, \delta, \delta) \right) [\beta_{t'} (1 - b\beta_t) \varrho_c - b\alpha_t \alpha_{t'}] \\
&+ \frac{1}{2} \nu(\varrho) \sum_{\epsilon, \iota}^r I_{\sigma'\sigma\sigma'\sigma}^{t,t',t',c}(\gamma, \epsilon, \delta, \iota) \mathcal{Q}_{\gamma\epsilon} \mathcal{Q}_{\delta\iota} [\beta_t \beta_{t'} \varrho_c + \alpha_t \alpha_{t'}] \\
&- \nu(\varrho) \sum_{\epsilon=1}^r \left((1 - b\beta_{t'}) I_{\sigma'\sigma\sigma'\lambda^1}^{t,t',c}(\gamma, \epsilon, \delta, \delta) - b\alpha_{t'} I_{\sigma'\sigma\sigma'\lambda^0}^{t,t',c}(\gamma, \epsilon, \delta, \delta) \right) \mathcal{Q}_{\epsilon\gamma} [\beta_t \beta_{t'} \varrho_c + \alpha_t \alpha_{t'}] \\
&+ \frac{1}{2} \left((1 - b\beta_{t'}) (1 - b\beta_t) I_{\sigma'\sigma'\lambda^1 \lambda^1}^{t,t',t',c}(\gamma, \delta, \gamma, \delta) - (1 - b\beta_{t'}) b\alpha_t I_{\sigma'\sigma'\lambda^0 \lambda^1}^{t,t',t',c}(\gamma, \delta, \gamma, \delta) \right) \\
&- b\alpha_{t'} (1 - b\beta_t) I_{\sigma'\sigma'\lambda^0 \lambda^1}^{t,t',t',c}(\gamma, \delta, \delta, \gamma) + b^2 \alpha_t \alpha_{t'} I_{\sigma'\sigma'\lambda^0 \lambda^0}^{t,t',t',c}(\gamma, \delta, \gamma, \delta) \nu(\varrho) (\beta_t \beta_{t'} \varrho_c + \alpha_t \alpha_{t'}) \\
&+ (\gamma \leftrightarrow \delta)
\end{aligned} \tag{59}$$

We introduced the integrals

$$I_{\sigma\sigma}^{t,t',c}(\gamma, \delta) = \mathbb{E}_{\omega_\gamma, \omega_\delta} [\sigma(\omega_\gamma)\sigma(\omega_\delta)]$$

$$\omega_\gamma, \omega_\delta \sim \mathcal{N}\left((\beta_t, \beta_{t'}) \odot M_{(\gamma, \delta)}^c, \Omega_{(\gamma, \delta)}^{t,t',c}\right) \quad (60)$$

$$I_{\sigma\sigma\sigma'}^{t_1, t_2, t_3, c}(\gamma, \epsilon, \delta) = \mathbb{E}_{\omega_\gamma, \omega_\epsilon, \omega_\delta} [\sigma(\omega_\gamma)\sigma(\omega_\epsilon)\sigma'(\omega_\delta)],$$

$$\omega_\gamma, \omega_\epsilon, \omega_\delta \sim \mathcal{N}\left((\beta_{t_1}, \beta_{t_2}, \beta_{t_3}) \odot M_{(\gamma, \epsilon, \delta)}^c, \Omega_{(\gamma, \epsilon, \delta)}^{(3), t_1, t_2, t_3, c}\right) \quad (61)$$

$$I_{\sigma\sigma'\lambda^1}^{t_1, t_2, t_3, c}(\gamma, \epsilon, \delta) = \mathbb{E}_{\omega_\gamma, \omega_\epsilon, \lambda_\delta^1} [\sigma(\omega_\gamma)\sigma'(\omega_\epsilon)\lambda_\delta^1],$$

$$\omega_\gamma, \omega_\epsilon, \lambda_\delta^1 \sim \mathcal{N}\left((\beta_{t_1}, \beta_{t_2}, 1) \odot M_{(\gamma, \epsilon, \delta)}^c, \Phi_{(\gamma, \epsilon, \delta)}^{(3), t_1, t_2, t_3, c}\right) \quad (62)$$

$$I_{\sigma\sigma'\lambda^0}^{t_1, t_2, t_3, c}(\gamma, \epsilon, \delta) = \mathbb{E}_{\omega_\gamma, \omega_\epsilon, \lambda_\delta^0} [\sigma(\omega_\gamma)\sigma'(\omega_\epsilon)\lambda_\delta^0],$$

$$\omega_\gamma, \omega_\epsilon, \lambda_\delta^0 \sim \mathcal{N}\left((\beta_{t_1}, \beta_{t_2}, 0) \odot M_{(\gamma, \epsilon, \delta)}^c, \Psi_{(\gamma, \epsilon, \delta)}^{(3), t_1, t_2, t_3, c}\right) \quad (63)$$

$$I_{\sigma'\sigma'\sigma}^{t_1, t_2, t_3, t_4, c}(\gamma, \epsilon, \delta, \iota) = \mathbb{E}_{\omega_\gamma, \omega_\epsilon, \omega_\delta, \omega_\iota} [\sigma'(\omega_\gamma)\sigma(\omega_\epsilon)\sigma'(\omega_\delta)\sigma(\omega_\iota)]$$

$$\omega_\gamma, \omega_\epsilon, \omega_\delta, \omega_\iota \sim \mathcal{N}\left((\beta_{t_1}, \beta_{t_2}, \beta_{t_3}, \beta_{t_4}) \odot M_{(\gamma, \epsilon, \delta, \iota)}^c, \Omega_{(\gamma, \epsilon, \delta, \iota)}^{(4), t_1, t_2, t_3, t_4, c}\right) \quad (64)$$

$$I_{\sigma'\sigma'\lambda^1}^{t_1, t_2, t_3, t_4, c}(\gamma, \epsilon, \delta, \iota) = \mathbb{E}_{\omega_\gamma, \omega_\epsilon, \omega_\delta, \lambda_\iota^1} [\sigma'(\omega_\gamma)\sigma(\omega_\epsilon)\sigma'(\omega_\delta)\lambda_\iota^1]$$

$$\omega_\gamma, \omega_\epsilon, \omega_\delta, \lambda_\iota^1 \sim \mathcal{N}\left((\beta_{t_1}, \beta_{t_2}, \beta_{t_3}, 1) \odot M_{(\gamma, \epsilon, \delta, \iota)}^c, \Phi_{(\gamma, \epsilon, \delta, \iota)}^{(4), t_1, t_2, t_3, t_4, c}\right) \quad (65)$$

$$I_{\sigma'\sigma'\lambda^0}^{t_1, t_2, t_3, t_4, c}(\gamma, \epsilon, \delta, \iota) = \mathbb{E}_{\omega_\gamma, \omega_\epsilon, \omega_\delta, \lambda_\iota^0} [\sigma'(\omega_\gamma)\sigma(\omega_\epsilon)\sigma'(\omega_\delta)\lambda_\iota^0]$$

$$\omega_\gamma, \omega_\epsilon, \omega_\delta, \lambda_\iota^0 \sim \mathcal{N}\left((\beta_{t_1}, \beta_{t_2}, \beta_{t_3}, 0) \odot M_{(\gamma, \epsilon, \delta, \iota)}^c, \Psi_{(\gamma, \epsilon, \delta, \iota)}^{(4), t_1, t_2, t_3, t_4, c}\right) \quad (66)$$

$$I_{\sigma'\sigma'\lambda^1\lambda^1}^{t_1, t_2, t_3, t_4, c}(\gamma, \epsilon, \delta, \iota) = \mathbb{E}_{\omega_\gamma, \omega_\epsilon, \lambda_\delta^1, \lambda_\iota^1} [\sigma'(\omega_\gamma)\sigma'(\omega_\epsilon)\lambda_\delta^1\lambda_\iota^1]$$

$$\omega_\gamma, \omega_\epsilon, \lambda_\delta^1, \lambda_\iota^1 \sim \mathcal{N}\left((\beta_{t_1}, \beta_{t_2}, 1, 1) \odot M_{(\gamma, \epsilon, \delta, \iota)}^c, P_{(\gamma, \epsilon, \delta, \iota)}^{(4, 1, 1), t_1, t_2, t_3, t_4, c}\right) \quad (67)$$

$$I_{\sigma'\sigma'\lambda^0\lambda^1}^{t_1, t_2, t_3, t_4, c}(\gamma, \epsilon, \delta, \iota) = \mathbb{E}_{\omega_\gamma, \omega_\epsilon, \lambda_\delta^0, \lambda_\iota^1} [\sigma'(\omega_\gamma)\sigma'(\omega_\epsilon)\lambda_\delta^0\lambda_\iota^1]$$

$$\omega_\gamma, \omega_\epsilon, \lambda_\delta^0, \lambda_\iota^1 \sim \mathcal{N}\left((\beta_{t_1}, \beta_{t_2}, 0, 1) \odot M_{(\gamma, \epsilon, \delta, \iota)}^c, P_{(\gamma, \epsilon, \delta, \iota)}^{(4, 0, 1), t_1, t_2, t_3, t_4, c}\right) \quad (68)$$

$$I_{\sigma'\sigma'\lambda^0\lambda^0}^{t_1, t_2, t_3, t_4, c}(\gamma, \epsilon, \delta, \iota) = \mathbb{E}_{\omega_\gamma, \omega_\epsilon, \lambda_\delta^0, \lambda_\iota^0} [\sigma'(\omega_\gamma)\sigma'(\omega_\epsilon)\lambda_\delta^0\lambda_\iota^0]$$

$$\omega_\gamma, \omega_\epsilon, \lambda_\delta^0, \lambda_\iota^0 \sim \mathcal{N}\left((\beta_{t_1}, \beta_{t_2}, 0, 0) \odot M_{(\gamma, \epsilon, \delta, \iota)}^c, P_{(\gamma, \epsilon, \delta, \iota)}^{(4, 0, 0), t_1, t_2, t_3, t_4, c}\right) \quad (69)$$

We further denoted

$$\begin{aligned}
\Omega^{t,t',c} &= \alpha_t \alpha_{t'} \mathcal{Q} + \beta_t \beta_{t'} Q^c \\
\Omega_{(\gamma,\epsilon,\delta)}^{(3),t_1,t_2,t_3,c} &= \begin{pmatrix} \Omega_{\gamma\gamma}^{t_1,t_1,c} & \Omega_{\gamma\epsilon}^{t_1,t_2,c} & \Omega_{\gamma\delta}^{t_1,t_3,c} \\ \Omega_{\epsilon\gamma}^{t_2,t_1,c} & \Omega_{\epsilon\epsilon}^{t_2,t_2,c} & \Omega_{\epsilon\delta}^{t_2,t_3,c} \\ \Omega_{\delta\gamma}^{t_3,t_1,c} & \Omega_{\delta\epsilon}^{t_3,t_2,c} & \Omega_{\delta\delta}^{t_3,t_3,c} \end{pmatrix} \\
\Phi_{(\gamma,\epsilon,\delta)}^{(3),t_1,t_2,t_3,c} &= \begin{pmatrix} \Omega_{\gamma\gamma}^{t_1,t_1,c} & \Omega_{\gamma\epsilon}^{t_1,t_2,c} & \beta_{t_1} Q_{\gamma\delta}^c \\ \Omega_{\epsilon\gamma}^{t_2,t_1,c} & \Omega_{\epsilon\epsilon}^{t_2,t_2,c} & \beta_{t_2} Q_{\epsilon\delta}^c \\ \beta_{t_1} Q_{\gamma\delta}^c & \beta_{t_2} Q_{\epsilon\delta}^c & Q_{\delta\delta}^c \end{pmatrix} \\
\Psi_{(\gamma,\epsilon,\delta)}^{(3),t_1,t_2,t_3,c} &= \begin{pmatrix} \Omega_{\gamma\gamma}^{t_1,t_1,c} & \Omega_{\gamma\epsilon}^{t_1,t_2,c} & \alpha_{t_1} \mathcal{Q}_{\gamma\delta} \\ \Omega_{\epsilon\gamma}^{t_2,t_1,c} & \Omega_{\epsilon\epsilon}^{t_2,t_2,c} & \alpha_{t_2} \mathcal{Q}_{\epsilon\delta} \\ \alpha_{t_1} Q_{\gamma\delta}^c & \alpha_{t_2} \mathcal{Q}_{\epsilon\delta} & \mathcal{Q}_{\delta\delta} \end{pmatrix} \\
\Omega_{(\gamma,\epsilon,\delta,\iota)}^{(4),t_1,t_2,t_3,t_4,c} &= \begin{pmatrix} \Omega_{\gamma\gamma}^{t_1,t_1,c} & \Omega_{\gamma\epsilon}^{t_1,t_2,c} & \Omega_{\gamma\delta}^{t_1,t_3,c} & \Omega_{\gamma\iota}^{t_1,t_4,c} \\ \Omega_{\epsilon\gamma}^{t_2,t_1,c} & \Omega_{\epsilon\epsilon}^{t_2,t_2,c} & \Omega_{\epsilon\delta}^{t_2,t_3,c} & \Omega_{\epsilon\iota}^{t_2,t_4,c} \\ \Omega_{\delta\gamma}^{t_3,t_1,c} & \Omega_{\delta\epsilon}^{t_3,t_2,c} & \Omega_{\delta\delta}^{t_3,t_3,c} & \Omega_{\delta\iota}^{t_3,t_4,c} \\ \Omega_{\gamma\iota}^{t_4,t_1,c} & \Omega_{\epsilon\iota}^{t_4,t_2,c} & \Omega_{\delta\iota}^{t_4,t_3,c} & \Omega_{\iota\iota}^{t_4,t_4,c} \end{pmatrix} \\
\Phi_{(\gamma,\epsilon,\delta,\iota)}^{(4),t_1,t_2,t_3,t_4,c} &= \begin{pmatrix} \Omega_{\gamma\gamma}^{t_1,t_1,c} & \Omega_{\gamma\epsilon}^{t_1,t_2,c} & \Omega_{\gamma\delta}^{t_1,t_3,c} & \beta_{t_1} Q_{\gamma\iota}^c \\ \Omega_{\epsilon\gamma}^{t_2,t_1,c} & \Omega_{\epsilon\epsilon}^{t_2,t_2,c} & \Omega_{\epsilon\delta}^{t_2,t_3,c} & \beta_{t_2} Q_{\epsilon\iota}^c \\ \Omega_{\delta\gamma}^{t_3,t_1,c} & \Omega_{\delta\epsilon}^{t_3,t_2,c} & \Omega_{\delta\delta}^{t_3,t_3,c} & \beta_{t_3} Q_{\delta\iota}^c \\ \beta_{t_1} Q_{\gamma\iota}^c & \beta_{t_2} Q_{\epsilon\iota}^c & \beta_{t_3} Q_{\delta\iota}^c & Q_{\iota\iota}^c \end{pmatrix} \\
\Psi_{(\gamma,\epsilon,\delta,\iota)}^{(4),t_1,t_2,t_3,t_4,c} &= \begin{pmatrix} \Omega_{\gamma\gamma}^{t_1,t_1,c} & \Omega_{\gamma\epsilon}^{t_1,t_2,c} & \Omega_{\gamma\delta}^{t_1,t_3,c} & \alpha_{t_1} \mathcal{Q}_{\gamma\iota} \\ \Omega_{\epsilon\gamma}^{t_2,t_1,c} & \Omega_{\epsilon\epsilon}^{t_2,t_2,c} & \Omega_{\epsilon\delta}^{t_2,t_3,c} & \alpha_{t_2} \mathcal{Q}_{\epsilon\iota} \\ \Omega_{\delta\gamma}^{t_3,t_1,c} & \Omega_{\delta\epsilon}^{t_3,t_2,c} & \Omega_{\delta\delta}^{t_3,t_3,c} & \alpha_{t_3} \mathcal{Q}_{\delta\iota} \\ \alpha_{t_1} \mathcal{Q}_{\gamma\iota} & \alpha_{t_2} \mathcal{Q}_{\epsilon\iota} & \alpha_{t_3} \mathcal{Q}_{\delta\iota} & \mathcal{Q}_{\iota\iota} \end{pmatrix} \\
P_{(\gamma,\epsilon,\delta,\iota)}^{(4,1,1),t_1,t_2,t_3,t_4,c} &= \begin{pmatrix} \Omega_{\gamma\gamma}^{t_1,t_1,c} & \Omega_{\gamma\epsilon}^{t_1,t_2,c} & \beta_{t_1} Q_{\gamma\delta}^c & \beta_{t_1} Q_{\gamma\iota}^c \\ \Omega_{\epsilon\gamma}^{t_2,t_1,c} & \Omega_{\epsilon\epsilon}^{t_2,t_2,c} & \beta_{t_2} Q_{\epsilon\delta}^c & \beta_{t_2} Q_{\epsilon\iota}^c \\ \beta_{t_1} Q_{\gamma\delta}^c & \beta_{t_2} Q_{\epsilon\delta}^c & Q_{\delta\delta}^c & Q_{\delta\iota}^c \\ \beta_{t_1} Q_{\gamma\iota}^c & \beta_{t_2} Q_{\epsilon\iota}^c & Q_{\iota\delta}^c & Q_{\iota\iota}^c \end{pmatrix} \\
P_{(\gamma,\epsilon,\delta,\iota)}^{(4,0,1),t_1,t_2,t_3,t_4,c} &= \begin{pmatrix} \Omega_{\gamma\gamma}^{t_1,t_1,c} & \Omega_{\gamma\epsilon}^{t_1,t_2,c} & \alpha_{t_1} \mathcal{Q}_{\gamma\delta} & \beta_{t_1} Q_{\gamma\iota}^c \\ \Omega_{\epsilon\gamma}^{t_2,t_1,c} & \Omega_{\epsilon\epsilon}^{t_2,t_2,c} & \alpha_{t_2} \mathcal{Q}_{\epsilon\delta} & \beta_{t_2} Q_{\epsilon\iota}^c \\ \alpha_{t_1} \mathcal{Q}_{\gamma\delta} & \alpha_{t_2} \mathcal{Q}_{\epsilon\delta} & \mathcal{Q}_{\delta\delta} & 0 \\ \beta_{t_1} Q_{\gamma\iota}^c & \beta_{t_2} Q_{\epsilon\iota}^c & 0 & Q_{\iota\iota}^c \end{pmatrix} \\
P_{(\gamma,\epsilon,\delta,\iota)}^{(4,0,0),t_1,t_2,t_3,t_4,c} &= \begin{pmatrix} \Omega_{\gamma\gamma}^{t_1,t_1,c} & \Omega_{\gamma\epsilon}^{t_1,t_2,c} & \alpha_{t_1} \mathcal{Q}_{\gamma\delta} & \alpha_{t_1} \mathcal{Q}_{\gamma\iota} \\ \Omega_{\epsilon\gamma}^{t_2,t_1,c} & \Omega_{\epsilon\epsilon}^{t_2,t_2,c} & \alpha_{t_2} \mathcal{Q}_{\epsilon\delta} & \alpha_{t_2} \mathcal{Q}_{\epsilon\iota} \\ \alpha_{t_1} \mathcal{Q}_{\gamma\delta} & \alpha_{t_2} \mathcal{Q}_{\epsilon\delta} & \mathcal{Q}_{\delta\delta} & \mathcal{Q}_{\delta\iota} \\ \alpha_{t_1} \mathcal{Q}_{\gamma\iota} & \alpha_{t_2} \mathcal{Q}_{\epsilon\iota} & \mathcal{Q}_{\iota\delta} & \mathcal{Q}_{\iota\iota} \end{pmatrix} \tag{70}
\end{aligned}$$

A.2.7 Continuous time limit

Equations (53),(55),(58) and (59) provide the update equations for the summary statistic densities $m(\cdot), g(\cdot), q(\cdot)$ under SGD steps (5), which take the form

$$\begin{aligned}
\frac{d}{2\eta} dm(\varrho) &= F_m(\varrho, m(\varrho), q(\varrho), M, Q, \mathcal{Q}, b), \\
\frac{d}{2\eta} dg &= F_g(\varrho, m(\varrho), q(\varrho), M, Q, \mathcal{Q}, b), \\
\frac{d}{2\eta} dq &= F_q(\varrho, m(\varrho), q(\varrho), M, Q, \mathcal{Q}, b), \tag{71}
\end{aligned}$$

where the update functions $F_{m,q,g}$ denote the right hand sides of (53),(55),(58) and (59), and we have omitted the time step indices to ease the notations. From (46), these updates translate directly at the level of the summary statistics M, Q, Ω, G into

$$\begin{aligned}
\frac{d}{2\eta}dM^c &= F_M(M, Q, \Omega, b)^c, & F_M(\cdot)^c &= \int F_m(\varrho, m(\varrho), q(\varrho), \cdot)^c d\varrho, \\
\frac{d}{2\eta}dG &= F_G(M, Q, \Omega, b), & F_G(\cdot) &= \int F_g(\varrho, m(\varrho), q(\varrho), \cdot) d\varrho, \\
\frac{d}{2\eta}dQ^c &= F_Q(M, Q, \Omega, b)^c, & F_Q(\cdot)^c &= \int \varrho_c F_q(\varrho, m(\varrho), q(\varrho), \cdot) d\varrho, \\
\frac{d}{2\eta}d\Omega &= F_\Omega(M, Q, \Omega, b), & F_\Omega(\cdot) &= \int F_q(\varrho, m(\varrho), q(\varrho), \cdot) d\varrho.
\end{aligned} \tag{72}$$

We remind that from (19), the skip connection strength similarly obeys

$$\frac{d}{2\eta}db = F_b(b), \tag{73}$$

where the update function F_b corresponds to the right hand side of equation (19). Now remark that in the asymptotic limit $d \rightarrow \infty$, the coefficient $d/2\eta$ tends to zero. Introducing the time variable $\vartheta \equiv 2\eta\mu/d$, so that $d\vartheta = 2\eta/d$, the discrete processes (72) and (73) are thus asymptotically described by the limiting ODEs

$$\begin{aligned}
\frac{dM}{d\vartheta} &= F_M(M, Q, \Omega, b), \\
\frac{dQ}{d\vartheta} &= F_Q(M, Q, \Omega, b), \\
\frac{d\Omega}{d\vartheta} &= F_\Omega(M, Q, \Omega, b), \\
\frac{db}{d\vartheta} &= F_b(b).
\end{aligned} \tag{74}$$

Finally, the last ODE, governing the dynamics of the skip connection strength b over the SGD optimization dynamics, can be solved in closed-form as

$$b(\vartheta) = \frac{\Lambda \mathbb{E}_t[\beta_t]}{\Lambda \mathbb{E}_t[\beta_t^2] + \mathbb{E}_t[\alpha_t^2]} \left[1 - e^{-(\Lambda \mathbb{E}_t[\beta_t^2] + \mathbb{E}_t[\alpha_t^2])\vartheta} \right] + b_0 e^{-(\Lambda \mathbb{E}_t[\beta_t^2] + \mathbb{E}_t[\alpha_t^2])\vartheta}, \tag{75}$$

where b_0 designates the value of b at initialization. This completes the derivation of Result 2.1. \square

A.3 Numerical validation

We plot the theoretical predictions of Result 2.1 for the evolution of the summary statistics M, Q, Ω, G, b (33) under the SGD dynamics (5) in Fig. 6 for a Gaussian mixture target density ρ with three isotropic modes, learnt by an AE with $r = 2$ hidden units and tanh activation, using learning rate $\eta = 0.2$ and weight decay $\lambda = 0$. The centroids of the clusters were taken as $\pm e_1, e_2$ for two orthonormal vectors e_1, e_2 , and the columns of the weight matrix w were initialized with a warm start as $0.1 \times e_{1,2}$. Finally, for simplicity, the expectation \mathbb{E}_t in (5) was chosen to bear over a delta distribution around $\mathcal{G} = \{1/2\}$, instead of the full integral over $[0, 1]$. Including more points in the grid \mathcal{G} was not found to significantly alter the qualitative aspect of the generated density. Fig. 6 reveals an overall good agreement between the theoretical predictions of Result 2.1 (dashed lines) and numerical experiments (solid lines), obtained by simulating the model in large but finite dimension $d = 1000$.

Fig. 7 similarly contrasts numerical experiments for a target distribution corresponding to MNIST images of sevens (dotted lines), a Gaussian target density with matching covariance (solid lines), and the theoretical predictions of Result 2.1 for the latter. All experimental details are specified in the caption. Although the agreement between the three curves is overall good, discrepancies appear, in particular due to the rather low dimensionality $d = 784$.

A.4 Extensions

We briefly describe, for completeness, how the analysis can be generalized to characterize the learning of more complex DAE architectures. Namely, we discuss how the derivation can be adapted to accommodate (a) untied weights and (b) time encodings.

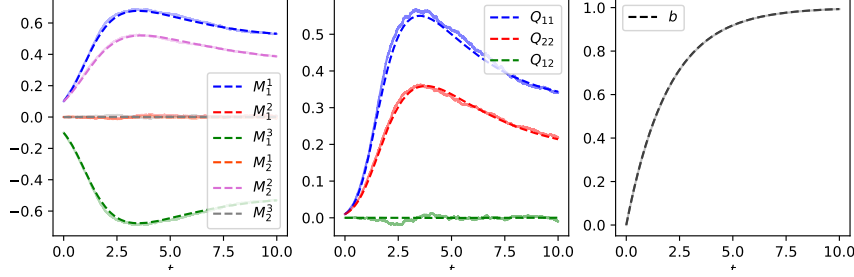


Figure 6: Evolution of the summary statistics (33) M (left), Q (middle) and skip connection strength b (right), characterizing the dynamics of the AE parameters (4) under SGD dynamics (5). Parameters $\sigma = \tanh, r = 2, \lambda = 0, \eta = 0.2, \mathcal{G} = \{1/2\}$ were used, and the target density ρ was taken to be a Gaussian mixture with three isotropic clusters (see also Fig. 1 in the main text). The weight vectors were initialized along the centroids of the target density, with norm 0.1, while the initial skip connection strength is $b_0 = 0$. Dashed lines: theoretical characterization of Result 2.1. Continuous lines: numerical experiments in $d = 1000$, for a single run.

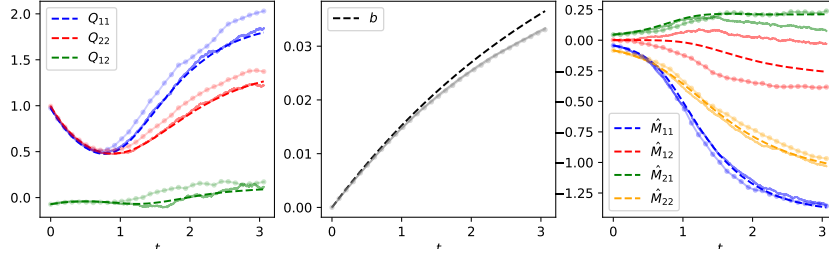


Figure 7: Evolution of the summary statistics (33) Q (left), b (middle) and skip connection strength M (right), characterizing the dynamics of the AE parameters (4) under SGD dynamics (5). Parameters $\sigma = \tanh, r = 2, \lambda = 0.784, \eta = 0.2, \mathcal{G} = \{1/2\}$ were used; weights were initialized with random independent Gaussian components and $b_0 = 0$. Dotted continuous lines : numerical experiments for a target density ρ given by the set of MNIST sevens. Continuous lines: numerical experiments for a unimodal Gaussian target distribution with covariance matching that of the set of MNIST sevens. Dashed lines: theoretical predictions of Result 2.1 for the latter Gaussian target density.

Untying the weights – The analysis reported in the present appendix can be extended to untied DAE architectures of the form

$$f_{b,u,v}(x) = b \times x + \frac{u}{\sqrt{d}} \sigma \left(\frac{v^\top x}{\sqrt{d}} \right), \quad (76)$$

trained with online SGD

$$b_{\mu+1} - b_\mu = -\frac{\eta}{d^2} \left(\partial_b \mathbb{E}_t \left\| x_1^\mu - f_{b_\mu, u_\mu, v_\mu} (\alpha_t x_0^\mu + \beta_t x_1^\mu) \right\|^2 \right), \quad (77)$$

$$u_{\mu+1} - u_\mu = -\eta \nabla_u \mathbb{E}_t \left\| x_1^\mu - f_{b_\mu, u_\mu, v_\mu} (\alpha_t x_0^\mu + \beta_t x_1^\mu) \right\|^2 - \eta \frac{\lambda}{d} u_\mu, \quad (78)$$

$$v_{\mu+1} - v_\mu = -\eta \nabla_v \mathbb{E}_t \left\| x_1^\mu - f_{b_\mu, u_\mu, v_\mu} (\alpha_t x_0^\mu + \beta_t x_1^\mu) \right\|^2 - \eta \frac{\lambda}{d} v_\mu. \quad (79)$$

Such an extension, however, comes at the price of more cumbersome expressions, as the summary statistics (33) needs to be introduced for the two sets of weights u, v , in addition to cross-statistics of the form $u^\top \Sigma(c)v/d$ and $u^\top v/d$. We refer the interested reader to Appendix B of [45] where such a derivation is detailed, in a closely related setting. Experimentally, in the probed settings, we did not observe a significant effect of (un)tying the weights on the qualitative phenomenology discussed in the main text.

Time encoding – As mentioned in the main text, the considered DAE parametrization (4) of the denoising function f (3) does not take into account the dependence of the latter on the sampling time t . To palliate this issue, a *time encoding* scheme is used in practice in order to include t as an input to the neural network. For the DAE architecture (4), a simple time encoding scheme consists in adding to the input x of the DAE the vector $e_t z$, for a fixed unit-norm vector $z \in \mathbb{R}^d$ and a function $e : [0, 1] \rightarrow \mathbb{R}$ of time. The SGD iteration then become

$$b_{\mu+1} - b_\mu = -\frac{\eta}{d^2} \left(\partial_b \mathbb{E}_t \left\| x_1^\mu - f_{b_\mu, w_\mu} (\alpha_t x_0^\mu + \beta_t x_1^\mu + e_t z) \right\|^2 \right), \quad (80)$$

$$w_{\mu+1} - w_\mu = -\eta \nabla_w \mathbb{E}_t \left\| x_1^\mu - f_{b_\mu, w_\mu} (\alpha_t x_0^\mu + \beta_t x_1^\mu + e_t z) \right\|^2 - \eta \frac{\lambda}{d} w_\mu, \quad (81)$$

and can be analyzed following nearly identical steps, modulo the introduction of the additional summary statistic $w^\top z/\sqrt{d}$. For the simple architecture considered here, the inclusion of such a time encoding was however not observed experimentally to have a significant impact on the observations discussed in the main text.

B Derivation of Result 2.2

In this section, we derive the tight characterization of Result 2.2 for the learnt generative transport process (7).

B.1 Generative SDE

We remind the generative SDE, leveraged to generate samples from $\hat{\rho}(t)$ starting from $X_0 \sim \mathcal{N}(0, \mathbb{I}_d)$:

$$\frac{dX_t}{dt} = \left(\dot{\beta}_t - \frac{\dot{\alpha}_t}{\alpha_t} \beta_t + \epsilon_t \frac{\beta_t}{\alpha_t^2} \right) f_{b_\tau, w_\tau}(X_t) + \left(\frac{\dot{\alpha}_t}{\alpha_t} - \frac{\epsilon_t}{\alpha_t^2} \right) X_t + \sqrt{2\epsilon_t} dW_t, \quad (82)$$

with W_t a Wiener process and ϵ_t the diffusion schedule. Introducing the shorthands

$$\Gamma_t = \dot{\beta}_t - \frac{\dot{\alpha}_t}{\alpha_t} \beta_t + \epsilon_t \frac{\beta_t}{\alpha_t^2} \quad (83)$$

$$\Delta_t^\tau = b_\tau \Gamma_t + \frac{\dot{\alpha}_t}{\alpha_t} - \frac{\epsilon_t}{\alpha_t^2}, \quad (84)$$

the generative SDE can be written more compactly as

$$\frac{dX_t}{dt} = \Delta_t^\tau X_t + \Gamma_t \frac{w_\tau}{\sqrt{d}} \sigma \left(\frac{w_\tau^\top X_t}{\sqrt{d}} \right) + \sqrt{2\epsilon_t} dW_t. \quad (85)$$

Importantly, note that the non-linear term $\sigma(\cdot)$ acts on the projection of X_t in the space \mathcal{W}_τ spanned by the columns of the trained weights matrix w_τ . Furthermore, its image also resides in \mathcal{W}_τ . In contrast, the dynamics in the orthogonal space \mathcal{W}_τ^\perp is simply linear. This motivates one to examine in succession the variable $Z_t \equiv w_\tau^\top X_t / \sqrt{d}$ and the projection $Y_t \equiv \Pi_{\mathcal{W}_\tau^\perp}^\perp X_t$ of X_t in \mathcal{W}_τ^\perp .

B.2 Dynamics in \mathcal{W}_τ

Let us first ascertain the evolution of Z_t , which tracks the evolution of a sample X_t in the weight space \mathcal{W}_τ . It follows directly from (85) that Z_t obeys the r -dimensional SDE

$$\frac{d}{dt} Z_t = \Delta_t^\tau Z_t + \Gamma_t Q_\tau \sigma(Z_t) + \sqrt{2\epsilon_t} Q^{1/2} dB_t, \quad (86)$$

with B_t a r -dimensional Wiener process, and Q_τ the summary statistic sharply characterized in Result 2.1. This recovers equation (14) of Result 2.2.

B.3 Dynamics in \mathcal{W}_τ^\perp

In \mathcal{W}_τ^\perp , the transport induced by the SDE (85) is simply linear:

$$\frac{dY_t}{dt} = \Delta_t^\tau Y_t + \sqrt{2\epsilon_t} dH_t, \quad (87)$$

with H_t here a $(d-r)$ -dimensional Wiener process. This SDE admits a compact closed-form solution

$$Y_t = e^{\int_0^t ds \Delta_s^\tau} Y_0 + e^{\int_0^t ds \Delta_s^\tau} \int_0^t e^{-\int_0^s dh \Delta_h^\tau} \sqrt{2\epsilon_s} dW_s. \quad (88)$$

By Itô isometry, Y_t is Gaussian with law

$$Y_t \sim \mathcal{N} \left(0_{\mathcal{W}_\tau^\perp}, e^{2 \int_0^t ds \Delta_s^\tau} \left[1 + 2 \int_0^t e^{-\int_0^s dh \Delta_h^\tau} \epsilon_s ds \right] \Pi_{\mathcal{W}_\tau^\perp}^\perp \right), \quad (89)$$

which recovers equation (15). This completes the derivation of Result 2.2. \square

B.4 Discretized sampling

As a final remark, let us note that the derivation presented in the present Appendix can be carried out in completely unchanged fashion starting from any discretization of the generative SDE (1). Let $t_0 = 0, t_1, \dots, t_T \in (0, 1)$ and consider the discrete stochastic process for $k \in \llbracket 0, T-1 \rrbracket$:

$$X_{k+1} - X_k = (t_{k+1} - t_k) \left[\left(\dot{\beta}_{t_k} - \frac{\dot{\alpha}_{t_k}}{\alpha_{t_k}} \beta_{t_k} + \epsilon_{t_k} \frac{\beta_{t_k}}{\alpha_{t_k}^2} \right) f_{b_\tau, w_\tau}(X_k) + \left(\frac{\dot{\alpha}_{t_k}}{\alpha_{t_k}} - \frac{\epsilon_{t_k}}{\alpha_{t_k}^2} \right) X_k + \sqrt{2\epsilon_{t_k}(t_{k+1} - t_k)} \xi_k \right], \quad (90)$$

starting from $X_{t_0} \sim \mathcal{N}(0, \mathbb{I}_d)$. In (90), $\xi_k \sim \mathcal{N}(0, \mathbb{I}_d)$ independently for each step k . Then the following version of Result 2.2 holds:

Result B.1. (Discrete dynamics) Consider a discretization $t_1, \dots, t_T \in (0, 1)$ and the discretized sampling process $(X_k)_{k \in \llbracket 1, T \rrbracket}$ (90). Denote $Y_k = \Pi_{\mathcal{W}_\tau^\perp}^\perp X_k$ and $Z_k = w_\tau^\top X_k / \sqrt{d}$, for a process X_k satisfying the generative process (90) from an initialization $X_0 \sim \mathcal{N}(0, \mathbb{I}_d)$. Then Z_t follows the low-dimensional stochastic process

$$Z_{k+1} - Z_k = (t_{k+1} - t_k) \left[\Delta_{t_k}^\tau Z_t + \Gamma_{t_k} Q_\tau \sigma(Z_k) \right] + \sqrt{2\epsilon_{t_k}(t_{k+1} - t_k)} Q_\tau^{1/2} \zeta_k, \quad (91)$$

from an initial condition $Z_0 \sim \mathcal{N}(0, Q_\tau)$, with $\zeta_k \sim \mathcal{N}(0, \mathbb{I}_r)$ and $\mathbb{E}[\zeta_k \zeta_l^\top] = \delta_{kl} \mathbb{I}_r$. On the other hand, Y_k is independently Gaussian-distributed as

$$Y_k \sim \mathcal{N} \left(0_{\mathcal{W}_\tau^\perp}, \left[\prod_{j=0}^{k-1} \left(1 + (t_{j+1} - t_j) \Delta_{t_j}^\tau \right)^2 + \sum_{j=0}^{k-2} 2\epsilon_{t_j} (t_{j+1} - t_j) \prod_{l=j+1}^{k-1} \left(1 + (t_{j+1} - t_j) \Delta_{t_j}^\tau \right)^2 + 2\epsilon_{t_{k-1}} (t_k - t_{k-1}) \right] \Pi_{\mathcal{W}_\tau^\perp}^\perp \right). \quad (92)$$

C Derivation of Corollary 2.3

Result 2.2 already provides a tight asymptotic characterization of the law of a sample X_t in terms of its projection Z_t (14) in the weights space \mathcal{W}_τ (characterized by a r -dimensional ODE) and its Gaussian component Y_t (15) in the orthogonal space \mathcal{W}_τ^\perp . A weakness of this characterization, however, lies in that it relies on a *training-time dependent* space \mathcal{W}_τ , with respect to which the characterization is formulated. Intuitively, this space rotates and changes as the model is further trained, making the result rather unwieldy. To palliate this shortcoming, one would rather select a *fixed, τ -independent*, reference subspace \mathcal{E} of finite dimension $R = \Theta_d(1)$, and transfer the characterization of Result 2.2 to this fixed subspace. Formally, this means ascertaining the law of the projection of X_t in \mathcal{E} , from that of its projections in $\mathcal{W}_\tau, \mathcal{W}_\tau^\perp$. This constitutes the objective of the present Appendix.

Let us fix an orthonormal basis $\{e_j\}_{j=1}^R$ of \mathcal{E} , stacked vertically in the matrix $E \in \mathbb{R}^{d \times R}$. We remind that we aim at characterizing the law of $E^\top X_t$. To that end, for any $1 \leq j \leq R$, start from the decomposition

$$e_j^\top X_t = (\Pi_{\mathcal{W}_\tau} e_j)^\top (\Pi_{\mathcal{W}_\tau} X_t) + e_j^\top \Pi_{\mathcal{W}_\tau}^\perp Y_t, \quad (93)$$

where we decomposed X_t into its projections in $\mathcal{W}_\tau, \mathcal{W}_\tau^\perp$. Note that, from Result 2.2 the two terms of this decomposition are independent. In the following, we sequentially ascertain the distribution of each of the terms in the decomposition (93).

C.1 Law of $(\Pi_{\mathcal{W}_\tau} e_j)^\top (\Pi_{\mathcal{W}_\tau} X_t)$

To compute $(\Pi_{\mathcal{W}_\tau} e_j)^\top (\Pi_{\mathcal{W}_\tau} X_t)$, we first aim to decompose e_j, X_t in a basis of \mathcal{W}_τ . Let us consider the eigendecomposition of the summary statistic $Q_\tau = w_\tau^\top w_\tau / d$ (characterized in Result 2.3) as

$$Q_\tau = U_\tau S_\tau U_\tau^\top. \quad (94)$$

This means that $B_\tau = 1/\sqrt{d}(S_\tau^+)^{1/2} U_\tau^\top w_\tau^\top$ forms a set of r orthonormal vectors (or a set of orthonormal vectors plus zero vectors if Q_τ is rank deficient), which we will use as a basis. We denoted S_τ^+ the Moore-Penrose pseudo-inverse of S_τ . The components of the reference vectors $E \in \mathbb{R}^{d \times R}$ (with columns $\{e_j\}$) and X_t in this basis are then given by

$$B_\tau E = \frac{1}{\sqrt{d}} (S_\tau^+)^{1/2} U_\tau^\top w_\tau^\top E = (S_\tau^+)^{1/2} U_\tau^\top G_\tau^\top \quad (95)$$

$$B_\tau X_t = \frac{1}{\sqrt{d}} (S_\tau^+)^{1/2} U_\tau^\top w_\tau^\top X_t = (S_\tau^+)^{1/2} U_\tau^\top Z_t, \quad (96)$$

where Z_t is characterized in Result 2.2. Then, very simply, the decomposition of X_t in the reference basis E restricted to \mathcal{W}_τ reads

$$(\Pi_{\mathcal{W}_\tau} e_j)^\top (\Pi_{\mathcal{W}_\tau} X_t) = e_j^\top B_\tau^\top B_\tau X_t = G_\tau Q_\tau^+ Z_t \quad (97)$$

C.2 Law of $E^\top \Pi_{\mathcal{W}_\tau}^\perp Y_t$

In distribution, $E^\top \Pi_{\mathcal{W}_\tau}^\perp Y_t$ inherits the Gaussianity of Y_t , as established in Result 2.2. It has mean zero and covariance

$$\begin{aligned} e^{2 \int_0^t ds \Delta_s^\tau} E^\top \Pi_{\mathcal{W}_\tau}^\perp E &= e^{2 \int_0^t ds \Delta_s^\tau} E^\top (\mathbb{I}_d - B_\tau^\top B_\tau) E \\ &= e^{2 \int_0^t ds \Delta_s^\tau} \left[\mathbb{I}_R - G_\tau Q_\tau^+ G_\tau^\top \right]. \end{aligned} \quad (98)$$

C.3 Law of $E^\top X_t$

One is now in a position to ascertain the law of $E^\top X_t$. Putting the above results together, in distribution:

$$E^\top X_t \stackrel{d}{=} G_\tau Q_\tau^+ Z_t + \mathcal{N} \left(0_R, e^{2 \int_0^t ds \Delta_s^\tau} \left[\mathbb{I}_R - G_\tau Q_\tau^+ G_\tau^\top \right] \right), \quad (99)$$

which recovers Corollary 2.3. \square

D Additional details on the numerical experiments

In this Appendix, we provide further specifications on the numerical experiments illustrated in Fig. 1, 3 and Fig. 5.

Generative process– In all the figures, the sampling was carried out by discretizing the interval $(0, 1)$ in 49 steps $t_k = 0.02 \times k$ for $k \in \llbracket 0, 49 \rrbracket$, and using the discretized SDE (90) in experiments, and the associated theoretical characterization of Results B.1 and 2.3 for the theoretical predictions. Note that we chose not to perform the last (50th) step, as the terms $1/\alpha_{t_k}$ in the sampling process diverge as t_k approaches 1, resulting in worsened performances and instabilities. Remark however that this is an experimental choice, and still falls in the range of applicability of Result B.1, and is thus still fully theoretically characterized.

Discretization of the manifold density π – In the generic case where $\pi(\cdot)$ (8) is not discrete, the ODE updates (10) still involve an integral over $d\pi(c)$, with c spanning \mathbb{R}^κ . For instance, in the setting of Fig. 5, at generation $g = 2$, $\kappa = r = 2$ and $\pi(c) = \Pi_{\mathcal{W}_\tau^{(1)}} \hat{\rho}^{(1)}(c)$. The latter is however still characterized in terms of a SDE (14), and not in closed-form. As a first step, we thus generated 4000 samples from π , using the theoretical characterization of Result 2.2, and approximated the density using the `scipy` [63] implementation of Gaussian kernel density estimation (KDE), in order to access a smooth estimation of π . The bandwidth was elected to be 1.5 times that determined using the Silverman method [56]. To perform the integral with measure $d\pi(c)$, we discretized π over a 10×10 grid, restricting the support to $[-1.5, 1.5] \times [-2.5, 2.5]$ where almost all of its mass was found to lie. The relative weights of the $10 \times 10 = 100$ discretized points were then evaluated from the KDE estimation, and overall normalization was finally enforced to ensure the relative weights sum to 1. Finally, this discretization was used in evaluating the theoretical characterization of Result 2.1, replacing the integrals over π by finite sums over the 100 points of the discretization. All results have been observed to be rather robust with respect to the choice of discretization, range, and bandwidth.

Preprocessing of the MNIST images– Finally, we detail the procedure used to evaluate the covariance of MNIST sevens used in Fig. 3. The total MNIST training set was used, retaining only sevens. The data was vectorized (flattened), centered, and normalized by 300. The empirical covariance was finally evaluated over the entire dataset, and used to generate the Gaussian target density considered in Fig. 3.